Design of Enoyl Acyl Carrier Protein Reductase inhibitors of *Tuberculosis Mycobacterium*, which can be administered orally and have a favorable pharmacokinetic profile.

ABSTRACT

Tuberculosis (TB) is a deep public health concern worldwide worsened by reported multidrug-resistant (MDR) and extensivelydrug-resistant (XDR) strains of *Mycobacterium tuberculosis*, the causative agent of the disease. A new class of thiadiazole inhibitors were reported to inhibit the enoyl-acyl transporter protein reductase (InhA) of *Mycobacterium tuberculosis* (*MTb*).We performed here the computer-aided molecular design of novel thiadiazole (TDZ) inhibitors of InhA by *in situ*modifying the reference crystal structure of (S)-1-(5-((1-(2,6-difluorobenzyl)-1*H*-pyrazol-3-yl)amino)-1,3,4-thiadiazol-2-yl)-1-(4-methylthiazol-2-yl)ethanol-InhA (PDB code: 4BQP). Thus a training set of 15 hybrids with known inhibition potency (IC_{50}^{exp}) was selected to establish a one-descriptor quantitative structure-activity relationship (QSAR) model resulting in a linear correlation between the Gibbs free energy (GFE) during the formation of the InhA-TDZ complex and IC_{50}^{exp}: pIC_{50}^{exp} = - $0.29 \times \Delta\Delta G_{com}$ + 7.66; R^2 = 0.92. The 3D pharmacophore model (PH4) generated from the active conformations of TDZs (pIC_{50}^{exp} = 0.93× pIC_{50}^{pred} + 0.47; R^2 = 0.94) served as a virtual screening tool for new analogs from a virtual library (VL). The combination of molecular modeling and PH4 *in silico* screening of VL resulted in the identification of novel potent antitubercular agent candidates with favorable pharmacokinetic profiles of which the six best hits predicted inhibitory potencies IC_{50}^{pre} in the sub nanomolar range (0.1 – 0.2 nM).

Keywords: Tuberculosis;enoyl-acyl carrier protein reductase (InhA); molecular modeling; QSAR models; pharmacophore; combinatorial library; ADME properties prediction.

1. INTRODUCTION

Tuberculosis is an ancient disease**[1]** caused by Kock's basil **[2]** which is transmitted from an affected subject to a healthy one through airborne contamination. 90% of the affected population are adults with more male than female. According to the 2022 WHO report **[3]**, 10.6 million people developed the disease in 2021 (i.e. 4.5% increase compared to 2020) with 1.6 million people dying from tuberculosis (including 187.000 among HIV-positive people). Clearly the pathogen is resistant to the various treatments administered. Multidrug-resistant tuberculosis (MDR-TB) is defined as an infection with the resistant strain of *Mycobacterium tuberculosis* (*MTb*) to the two first-line antimycobacterial drugs: isoniazid and rifampicin. Extensively drug-resistant tuberculosis (XDR-TB) is caused by a strain that is additionally resistant to at least three of the six second-line classes consisting of aminoglycosides, polypeptides, fluoroquinolones, thioamides, cycloserine, and para-aminosalicylicacid **[4]**. The term totally resistant (TDR-TB) has emerged to mean infection with a strain resistant to all first- and second-line drugs **[5]**. Used in clinical for more than half a century, and in the face of the various resistances of the various pathogenic strains to first and second line antimycobacterial drugs, it is more than urgent to find new drugs. These new inhibitors should be able to overcome all resistant strains, with a mechanism of action that shortens the duration of treatment, having a good pharmacokinetic profile for a lower dosing frequency, and having the shortest list of side effects and drug interactions **[6]**. Bedaquiline, a new antimycobacterial, approved at the end of 2012 **[7]** inhibits adenosine 5'-triphosphate (ATP)-synthase of *MTb* with good clinical efficacy against multiple resistant strains. However, this drug has cardiovascular side effects **[8]**.Fatty acids play an important role in the supply of metabolic precursors to biological membranes and represent an important form of metabolic energy production. Its synthesis is therefore an essential process for all living organisms. Mycobacteria contain both FAS I and FAS II fatty acid synthases.The enzymatic FAS II substrate specific to mycobacteria synthesizes mycolic acids which, bound to the cell wall, form a waxy substance of protective coating around the bacterial cell serving as a permeability barrier. This FAS fatty acid biosynthetic pathway in mycobacteria is a major target for the development of new antituberculotic agents **[9]**. Enoyl acyl carrier protein reductase (InhA) is a key component of the *M. tuberculosis* FAS II pathway. It is an NADH-dependent enzyme that facilitates the reduction of long-chain trans-2-enoyl-acyl carrier protein fatty acids (Figure 1) **[10].**InhA is made up of subunits including a central core which has a Rossmann fold containing the NADH binding site (Figure 1) **[11]**, several α-helices and β-strands of the Rossmann fold extending beyond the site binding of NADH, which creates a deep cleft for the lipophilic acyl substrate **[12]**.Isoniazid for its effectiveness must be converted, via a mycobacterial catalase-peroxidase (KatG) **[13]**, into an activated form of the drug **[14,15,16,17,18,19]**.This activated form believed to be an isonicotin-acyl radical covalently binds to the nicotinamide ring of NADH within the active site of InhA, creating an NADH adduct to form a reactive species that acylates the nicotinamide moiety of NADH **[13]**. Mutations in KatG are the main causes of resistance of mycobacteria to isoniazid. Compounds that can therefore directly inhibit InhA without the need for activation by KatG are of major interest in the fight against multidrug-resistant tuberculosis (MDR-TB), extensively drug-resistant tuberculosis (XDR-TB) and drug-resistant total tuberculosis (TDR-TB) **[20]**.Several

antituberculosis drugs have been explored such as triclosan and its derivatives **[21,22,23]**, pyrrolidine carboxamides **[24]**, benzamide derivatives **[25]**, and new polyketide synthases 13 **[26]**. A series of thiadiazole-based InhA inhibitors (TDZ) were discovered by GlaxoSmithKline in a high-throughput screening (Figure 1, B) **[27]**. The most active inhibitor obtained **TDZ1** is lipophilic, with a tetracyclic structure and a high proportion of sp2 centers and has been shown to be a direct and reversible inhibitor of InhA by binding in the active site, where it establishes contacts with NADH (IC_{50}^{exp} = 4 nM). Preliminary studies of structure-activity relationships were then made by AstraZeneca, where it was also shown that this binding depends on NADH oxidation **[27]**.Structural variations of this thiadiazole model are explored in the present study with the goal to assess new, more potent three-membered analogs that inhibit InhA and exhibit improved physicochemical properties for favorable pharmacokinetic profile. To do this, we used fifteen thiadiazole derivatives as the training set (TS) and three others as a validation set (VS) of inhibitors with their experimental inhibitory activities reported by Roman Sink et *al*. **[28]**.We have developed a complexation QSAR modelcorrelating the relative Gibbs free energy (rGFE) computed by simulating formation the fifteen InhA-$TDZ_{1\text{-}15}$ complexes built *in situ* (see § 2.2 Model Building) with their respective experimental inhibitory potencies (pIC_{50}^{exp}).Then a 3D-QSAR pharmacophore (PH4) model based on the fifteen active conformations from the complexation QSAR method has been generated as subsequent TDZ chemical subspace explorer. The subspace is an enumerated virtual library of TDZs analogues which, after screening using our PH4, yielded dozens hits mapping to most pharmacophoric features. Finally,the hits underwentcomplexation simulations for evaluationof the predicted inhibitory activity for the best analogues and for calculation of their ADME profile.

2. METHODS

2.1 Training and validation sets

The chemical structures and biological activities (IC_{50}^{exp}) of training and validation sets of InhA-inhibiting thiadiazoles used in this study come from the literature **[28]**. The potencies of these compounds cover a wide enough range of half-maximal inhibitory concentrations ($4 \leq IC_{50}^{exp} \leq 1003$ nM) to allow the construction of a QSAR model. The Training Set (TS) contains 15 TDZ inhibitors and the Validation Set (VS) includes 3 TDZs.

2.2 Model building

Three-dimensional (3D) molecular models of InhA-TDZx enzyme-inhibitor (E-I) complexes, free enzyme InhA and free inhibitors TDZx were prepared from the 1.89 Å resolution crystal structure of a reference complex containing the training set compound (S)-1-(5-((1-(2.6-difluorobenzyl)-1H-pyrazol-3-yl)ami-no)-1.3.4-thiadiazol-2-yl)-1-(4-methylthiazol-2-
yl) ethanol (TDZ-1) (Figure 1. B) bound to mycobacterial InhA (Protein Data Bank **[29]** PDB code: 4BQP **[28]**) using the molecular modeling program Insight- II **[30]**. The structures of InhA and E-I complexes were considered to be at pH 7 with N- and C-terminal residues and all protonizable and ionizable residues charged. No crystallographic water molecules were included in the model. The inhibitors were integrated into the 4BQP reference structure **[28]** by the *in situ* replacement of derived groups in the molecular scaffold of the matrix inhibitor TDZ1. Extensive conformational search of all rotational linkages of replacement function groups coupled with careful progressive minimization of the energy of the modified inhibitor and InhA active site residues located near the inhibitor (radius of 5 Å) was used to identify the low energy bound geometry of the modified inhibitor.

The resulting low-energy structures of the E-I complexes have been carefully refined by minimizing the entire complex. Successfully this procedure has been used for the construction of previous models of viral, bacterial and protozoan enzyme inhibitor complexes and the design of peptidomimetics, hydroxynaphthoic, thymidine, triclosan, pyrrolidine, carboxamides, nitriles, acid derivatives hydroxamic, benzofuran derivatives and chalcone-based inhibitors **[24,24,25,31 ,32,33,34,35,36,37**].

2.3 Molecular mechanics

Modeling of inhibitors, InhA and E-I complexes was carried out by molecular mechanics using CFF force field **[38]**.

2.4 Conformational search

Conformations of free inhibitors were derived from their bound conformations in E-I complexes by progressive relaxation to the nearest local energy minimum as previously described **[33]**.

2.5 Solvation Gibbsfree energies

The electrostatic component of the relative Gibbs free energy of solvation (rGFE) which also includes the effects of ionic strength via numerically solving the nonlinear Poisson-Boltzmann equation[**39**,**40**,**41]**was calculated by the DelPhi module in Discovery Studio [**42**].

2.6 Calculation of binding affinity and QSAR model

Calculation of binding affinity expressed as GFE complexation has been fully described above (see session **3-2-1**).

2.7 Interaction energy

Calculation of the MM interaction energy (E_{int}) between the enzyme residues and the inhibitor was performed as previously described **[33]**.

2.8 Pharmacophore generation

The bound conformations of the inhibitors taken from the E-I complex models were used for the construction of the 3D-QSAR (PH4) pharmacophore by means of the Catalyst HypoGen algorithm **[43]** implemented in Discovery Studio **[42]** as previously reported **[33]**.

2.9 ADME properties

The pharmacokinetic profile of BHMBs was calculated by the QikProp program **[44]** as described earlier **[33]**.

2.10 Virtual Library generation

The generation of the virtual library was performed as previously described **[3333]**.

2.11 ADME-Based library searching

The drug-likeness selection criterion served to focus the initial virtual library as described earlier **[33]**.

2.12 Pharmacophore-Based library searching

The pharmacophore model (PH4) described in section 4.8 and derived from the model related to the conformations of TDZs at the active site of InhA served as a library search tool as described earlier **[3333]**.

2.13 Inhibitory potency prediction

The conformer with the best mapping on the PH4 pharmacophore in each cluster of the focused library subset was selected for in silico screening by the complexation QSAR model. The computed $\Delta\Delta G_{com}$ of each selected new analog was used for prediction TDZ inhibitory potency ($\mathbf{IC_{50}^{pred}}$) of the focused virtual library of TDZ analog by inserting this parameter into the target-specific scoring function given in equation (1) parameterized using the complexation QSA model of the training set of TDZ inhibitors.

$$p\mathbf{IC_{50}^{pred}} = -\log_{10}\mathbf{IC_{50}^{pred}} = a.\ \Delta\Delta G_{com} + b \quad (1)$$

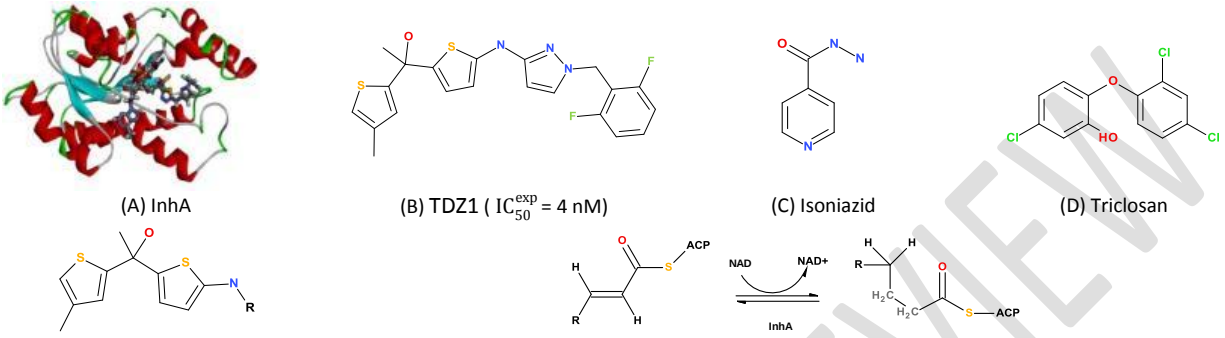

Figure 1: (A) Three-dimensional structure of InhA. (B) TDZ1 discovered by GlaxoSmithKline. (C) Chemical structure of Isoniazid. (D) Chemical structure of triclosan. (E) Scaffold atom and the substitution position of the R group. (F) Reaction catalyzed by InhA.

3. RESULTS

3.1 Training and validation sets of InhA inhibitors

The set of data including the chemical structures and the experi-mental biological activities of the thiadiazole derivatives, InhA inhibitors used in this work, is taken from the article published by Roman Sink et al. **[28]**. These compounds were divided into two groups including 15 for the test set (TS) and 3 for the validation set (VS) according to Table 1. They cover a range of half-maximal inhibitory concentrations (4 nM ≤ IC_{50}^{exp} ≤ 1003 nM) wide sufficiently to allow the design of a reliable QSAR model.

3.2 QSAR model of InhA inhibition

3.2.1 Single-descriptor QSAR model of InhA-TDZsaffinity

Each of the 15 TS and 3 VS InhA-TDZx complexes (Table 1), was prepared by *in situ* modification of the crystal structure of the refined matrix (PDB entry code **4PQP**) of the InhA-TDZ1 complex as described in the Methods section. In addition, the relative Gibbs free energy of formation of the InhA-TDZx complex ($\Delta\Delta G_{com}$) was calculated for each of the 18 enzyme-inhibitor complexes. Table 2 lists the calculated values of $\Delta\Delta G_{com}$ and its components ($\Delta\Delta H_{MM}$, $\Delta\Delta TS_{vib}$ and $\Delta\Delta G_{sol}$) for the TS and VS of thiadiazoles**[28]**. The QSAR model explained more than 92% of the variation in the experimental inhibitory powers of TDZs (pIC_{50}^{exp} = $-\log_{10}$ (IC_{50}^{exp}) **[28]**) by correlating it with $\Delta\Delta G_{com}$calcu-lated by linear regression (table 3). The QSAR model explained more than 92% of the variation in the experimental inhibitory powers of TDZs (pIC_{50}^{exp} =$-\log_{10}$ (IC_{50}^{exp}) **[28]**) by correlating it with $\Delta\Delta G_{com}$ calculated by linear regression (Table 3).

Table 1: Set (TDZ1-15) and validation set (TDZV1-3) of InhA inhibitors [30] used in the preparation of QSAR models of inhibitor binding.

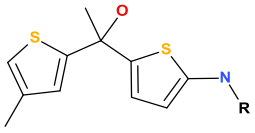

	TDZ**1**	TDZ**2**	TDZ**3**	TDZ**4**	TDZ**5**	TDZ**6**
R	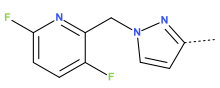	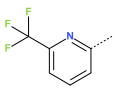	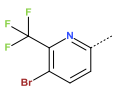	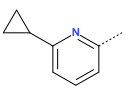	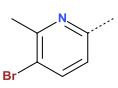	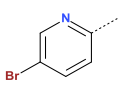
$\mathbf{IC_{50}^{exp}}$(nM)	4	18	46	77	179	197
	TDZ**7**	TDZ**8**	TDZ**9**	TDZ**10**	TDZ**11**	TDZ**12**

R		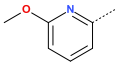			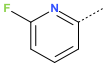	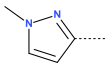
IC_{50}^{exp}(nM)	260	264	363	386	551	894
	TDZ**13**	TDZ**14**	TDZ**15**	TDZ**V1**	TDZ**V2**	TDZ**V3**
R	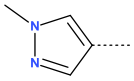	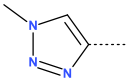		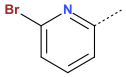	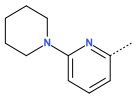	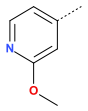
IC_{50}^{exp} (nM)	1001	1002	1003	13	299	741

Relatively high values of the R^2 regression coefficient, R^2_{xv} crossover validated regression coefficient, and Fischer's F-test of correlation in solvent suggest a strong relationship between the 3D model of inhibitor binding and inhibitory potencies observed from TDZs. In addition, the $pIC_{50}^{pre}/pIC_{50}^{exp}$ ≈1 ratio calculated for the entire VS validation set reinforces the robustness of our QSAR model. Therefore, the structural information derived from 3D models of the complexes can be expected to lead to a reliable prediction of the inhibitory potencies of InhA-TDZx for the new analogs based on the QSAR equation (B) (Table 3) as well than the generation of the pharmacophore PH4.

The statistical data confirmed validity of the correlation Equations (A) and (B) plotted on Figure 2. The ratio $pIC_{50}^{pre}/pIC_{50}^{exp}$ ≈1 (the pIC_{50}^{pre} values were estimated using correlation Equation B. Table 3) calculated for the validation set TDZV1-3 documents the substantial predictive power of the complexation QSAR model from Table 2. Thus, the regression Equation B (Table 3) and computed $\Delta\Delta G_{com}$ GFEs can be used for prediction of inhibitory potencies IC_{50}^{pre} against InhA for novel TDZ analogs, provided they share the same binding mode as the training set thiadiazole TDZ1-15.

3.3 Binding mode of TDZs

Structural information on enzyme-inhibitor interactions extracted from the crystal structure of the InhA-TDZ1 complex**[2828]**showedthatTDZs are specific inhibitors of InhA. Several interactions are highlighted at the active site by observing figure 3. The methyl-thiazole group of TDZ1 engages with the ribose group of the nicotinamide ring of the NAD cofactor through a hydrogen bond (HB) between the thiazole nitrogen and the ribose hydroxyl of the nicotinamide ring. This nitrogen acts as a hydrogen bond acceptor for the ribose hydroxyl of the NAD cofactor **[27]**. The catalytic residue Met98 establishes a hydrogen donor-acceptor bond pair with the ligand: the nitrogen of the thiadiazole ring and the amine "NH" located between the thiadiazole and pyrazole rings maintain an H bond respectively with the amide skeleton "NH and carbonyl "O" of the catalytic residue Met98. The orientation of this donor–acceptor hydrogen and the pairing of bonds provide an excellent opportunity for the introduction of the pyrazole linker which allows better access to the hydrophobic pocket for the difluorophenyl ring. This large hydrophobic pocket accommodates various fragments enriching in the same way the structural quality of new analogues with better inhibitory power. Furthermore, the thiadiazole, pyrazole and phenyl ring of the endogenous ligand wrap around the side chain of Met103. Fluorine interactions are observed with Ala198 and Met103 as well as a Pi-Sulfide bond established between the sulfur of the thiazole and Met199. Several alkyl and Pi-alkyl interactions are also visible.Thelarge hydrophobic pocket containing residues Met98, Gln100,Met103, Gly104, Phe149, Ala157, Tyr158, Lys+165, Thr196, Leu197, Ala198, Met199, Ile202,Ala206, Leu207, Ile215, Leu218 **[45]**remains the prominent interaction rooting the TDZs in InhA active site (Figure 3. C) confirming our recent reportedresults about triclosanstargeting the same enzyme, starting from complexation QSAR simulations and ending by Molecular Dynamics runs to confirm the best TCL analogues'active conformation stability [46].

3.4 Interaction energy

For the same TS used to establish the complexation QSAR model, the interaction energy (E_{int}) was computed through Molecular Mechanic MM. This energy was calculated between the enzyme residues and the inhibitor through a protocol available on Discovery Studio (DS) **[42]** which calculates the non-binding interactions (the Van der Waals and electrostatic terms) between a defined set of atoms. The calculations were performed using the CFF force field with a dielectric constant of 4.The results are presented in the diagram of figure 4depicting the individual energetic contributionfrom each InhA active site residue to E_{int}. The breakdown of interaction energy into individual contributions from active site residues is important in the selection of R-group substituents for enhancing the binding affinity of thiadiazole analogs with InhA and subsequently their inhibitory capacity. For the analysis, individual contributions to $E_{int}$are classified into three groups according to the level of activity of the training set's ligands: the most active (TDZ1-5), the moderately active (TDZ6-10) and the less active ligands (TDZ11-15) (Figure 4: (A), (B) and (C)). Comparing these contributions values lets identify the residues which contribution to the binding affinity is yet to be improved. After analysis, we notice that the level of contribution with respect to the interaction energies of the residues of the active site is almost the same for the three categories of inhibitors. Therefore, no better specific suggestions about the R-group substituentswithbinding affinity enhancing capacity emerge. Therefore the design of new thiadiazoleTDZs analogues trhough a combinatorial approach is adopted. Accordingly, we generated an *in silico* library of 7800 thiadiazole analogs to be screened using the Pharmacophore PH4 of InhA inhibition derived from the QSAR complexation model, as can be seen from the IE analysis (Figure 4).

Table 2: Gibbs free energy (binding affinity) and its components for the training set of InhA Inhibitors TDZ1-15 and validation set inhibitors TDZV1-3 **[28]**.

Training	M_w [b]	$\Delta\Delta H_{MM}$ [c]	$\Delta\Delta G_{sol}$ [d]	$\Delta\Delta TS_{vib}$ [e]	$\Delta\Delta G_{com}$ [f]	IC_{50}^{exp} [g]

Set [a]	[g.mol^{-1}]	[kcal.mol^{-1}]	[kcal.mol^{-1}]	[kcal.mol^{-1}]	[kcal.mol^{-1}]	[nM]
TDZ1	434	0	0	0	0	4
TDZ2	387	-2.16	2.45	-1.95	2.24	18
TDZ3	466	2.43	-2.06	-3.6	3.97	46
TDZ4	359	4.57	1.73	2.23	4.07	77
TDZ5	412	4.44	2.27	-0.41	7.12	179
TDZ6	398	7.24	-0.85	-0.66	7.04	197
TDZ7	333	4.5	2.23	1.1	5.63	260
TDZ8	349	3.13	2.51	0.22	5.42	264
TDZ9	337	5.42	2.15	0.08	7.49	363
TDZ10	319	6.32	1.93	1.55	6.74	386
TDZ11	337	4.47	2.54	-1.11	8.11	551
TDZ12	322	6.24	2.97	1	8.21	894
TDZ13	322	7.5	1.78	1.44	7.84	1001
TDZ14	323	8.28	1.74	1.3	8.73	1002
TDZ15	333	7.65	2.44	1.98	8.11	1003
Validation	**M_w** [b]	**$\Delta\Delta H_{MM}$** [c]	**$\Delta\Delta G_{sol}$** [d]	**$\Delta\Delta TS_{vib}$** [e]	**$\Delta\Delta G_{com}$** [f]	**pIC_{50}^{pre} / pIC_{50}^{exp}** [g]
Set [a]	[g.mol^{-1}]	[kcal.mol^{-1}]	[kcal.mol^{-1}]	[kcal.mol^{-1}]	[kcal.mol^{-1}]	
TDZV1	398	2.49	-0.89	-1.11	2.71	0.93
TDZV2	402	7.5	2.88	5.34	5.04	1.02
TDZV3	349	5.55	3	0.92	7.61	0.97

[a] for the chemical structures of the training set of inhibitors see Table 1; [b] M_w is the molar mass of inhibitors; [c] $\Delta\Delta H_{MM}$ is the relative enthalpic contribution to the GFE change related to E-I complex formation derived by MM; $\Delta\Delta H_{MM} \approx [E_{MM}\{E\text{-}I_x\} - E_{MM}\{I_x\}] - [E_{MM}\{E\text{-}I_{ref}\} - E_{MM}\{I_{ref}\}]$. I_{ref} is the reference inhibitor TDZ1; [d] $\Delta\Delta G_{sol}$ is the relative solvent effect contribution to the GFE change of E-I complex formation: $\Delta\Delta G_{sol} = [G_{sol}\{E\text{-}I_x\} - G_{sol}\{I_x\}] - [G_{sol}\{E\text{-}I_{ref}\} - G_{sol}\{I_{ref}\}]$; [e] $-\Delta\Delta TS_{vib}$ is the relative entropic contribution of inhibitor I_x to the GFE of E-I_x complex formation: $\Delta\Delta TS_{vib} = [TS_{vib}\{I_x\}E - TS_{vib}\{I_x\}] - [TS_{vib}\{I_{ref}\}E - TS_{vib}\{I_{ref}\}]$; [f] $\Delta\Delta G_{com}$ is the overall relative GFE change of E-I_x complex formation: $\Delta\Delta G_{com} \approx \Delta\Delta H_{MM} + \Delta\Delta G_{sol} - \Delta\Delta TS_{vib}$; [g] IC_{50}^{exp} is the experimental half-maximal inhibition concentration of InhA obtained from ref. **[28]**; ratio of predicted and experimental half-maximal inhibition concentrations $pIC_{50}^{pre}/pIC_{50}^{exp}$ ($pIC_{50}^{pre} = -\log_{10}IC_{50}^{pre}$) was predicted from computed $\Delta\Delta G_{com}$ using the regression equation for InhA shown in Table 3, B.

Table 3: Analysis of computed binding affinities $\Delta\Delta G_{com}$, its enthalpic component $\Delta\Delta H_{MM}$ and experimental half-maximal inhibitory concentrations $pIC_{50}^{exp} = -\log_{10}IC_{50}^{exp}$ of TDZs towards *Mt*InhA**[28].**

Statistical Data of Linear Regression	**A**	**B**
$pIC_{50}^{exp} = -0.21x\Delta\Delta H_{MM} + 7.66$ (A)		
$pIC_{50}^{exp} = = -0.29x\Delta\Delta G_{com} + 8.13$ (B)		
Number of compound n	15	15
Squared correlation coefficient of regression R^2	0.75	0.92
LOO cross-validated squared correlation coefficient R^2_{xv}	0.73	0.91
Standard error of regression σ	0.36	0.21
Statistical significance of regression. Fisher F-test	38.11	142.67
Level of statistical significance α	>95%	>95%
Range of activities IC_{50}^{exp} [nM]	4 - 1003	

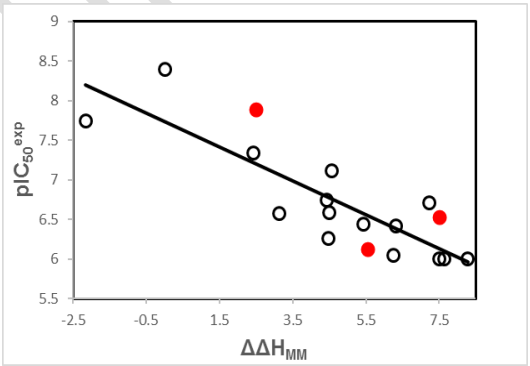

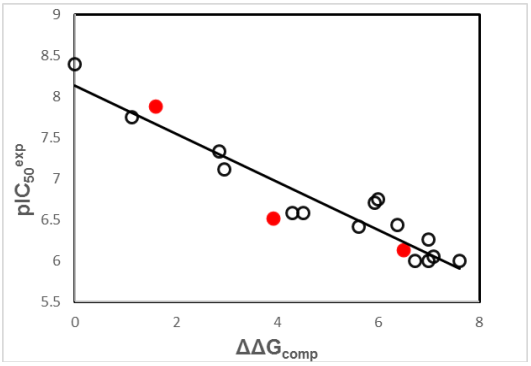

Figure 2: (**Top**) plot of correlation equation between pIC_{50}^{exp} and relative enthalpic contribution to the GFE ΔH_{MM} [kcal.mol^{-1}]. (**Bottom**) similar plot for relative complexation Gibbs free energies of the InhA-TDZxcomplex.formation$\Delta\Delta G_{com}$[kcal.mol^{-1}] of the training set **[28]**. The validation set data points are shown in red color.

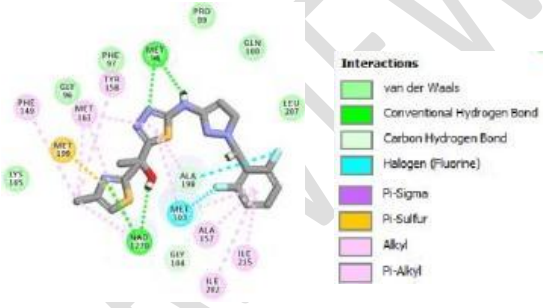

(A)

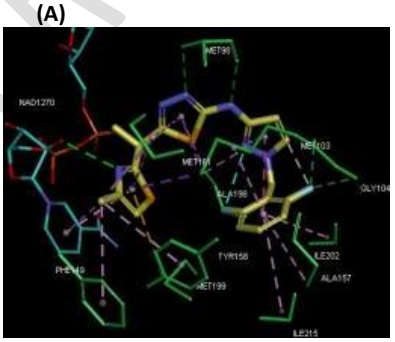

(B)

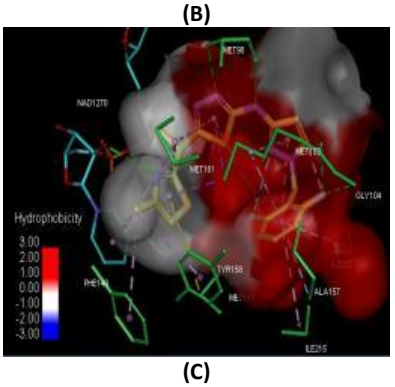

(C)

Figure 3: (A) 2D schematic interaction diagram of the most potent inhibitor TDZ1($IC_{50}^{exp} = 4$ nM) [**28**] at the active site of InhA. **(B)** 3D structure of the active site of InhA with the most active inhibitor TDZ1. The carbon atoms of the ligand are colored in yellow, the residues' side chains in green, NAD cofactor carbon atoms are in cyan. Interaction color code: hydrogen bonds (green), Alkyl and Pi-Alkyl (pink), Pi-Sulfide (orange), Fluorine bond (blue). **(C)** Molecular surface of the active site of InhA. Surface coloring legend: red, hydrophobic; blue, hydrophilic; white, intermediate.

3.5 3D-QSAR pharmacophore model

The interaction generation protocol in the Discovery Studio (DS) molecular modeling program **[42]** provides the pharmacophore characteristics of the active site of a protein.

3.5.1 InhA active site pharmacophore

The active site of InhA is globally hydrophobic (figure 3. C) as confirmed by previous work **[31,44]**. The design of competitive InhA substrate inhibitors often exploits the flexibility of the pocket due to the high mobility of the Tyr158, Phe149 side chains and the substrate-binding loop (Thr196–Gly208) **[47]**.

3.5.2 Generation and validation of 3D-QSAR pharmacophore

Through its algorithmic program Catalyst HypoGen [**43**], DS **[42]** allowed us to establish the active conformations of inhibitors from complexation QSAR models of different E-I complexes used for the construction of the 3D-QSAR pharmacophore (PH4). This construction made from the active conformation of 15 TS TDZ1-15 and evaluated by 3 VS TDZV1-3 covering a wide range of expe-

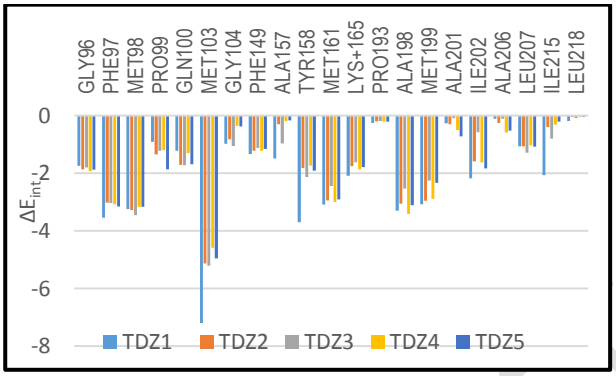

A

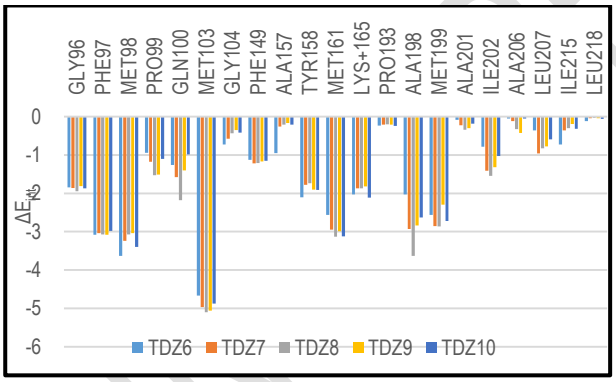

B

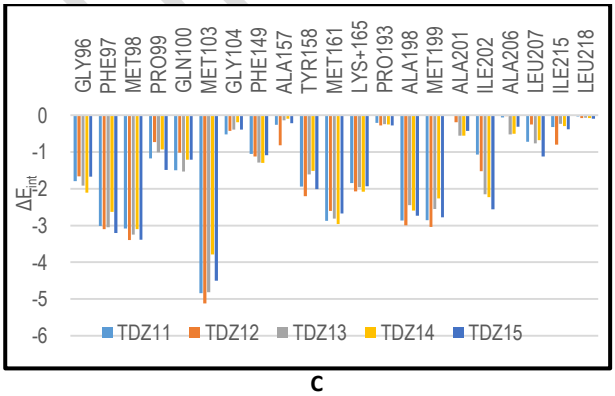

C

Figure 4: Mechanics of intermolecular interaction energy distribution of E_{int} to residue contributions in [kcal.mol^{-1}]: **(A)**Most active inhibitors TDZ1-5. **(B)** Moderately active inhibitors TDZ6-10. **(C)** Less active inhibitors TDZ11-15. Table 2 **[2828]**.

rimental activities (4–1003) nM was made in three steps: the constructive step, the subtractive step and the optimization step. During the build phase, as described earlier **[24],** only TDZ1 was automatically selected as the conductor to generate the starting PH4 features, as it alone fulfills the threshold criterion ($IC_{50}^{exp} \leq 1.25 \times 4$ nM = 5 nM). In the subtractive phase, compounds for which $IC_{50}^{exp} > 4{\times}10^{3.5}$ nM = 12649.1 nM were considered inactive. Consequently, none of the TDZx training sets were inactive and no starting PH4 functionality was removed. Finally, during the final optimization phase, the score of the PH4 hypotheses was improved. For the generation of the pharmacophore, four features available in the HypoGen algorithm were selected: aromatic hydrophobic (HYD_Ar), aliphatic hydrophobic (HYD_Al), hydrogen bond donor (HBD) and hydrogen bond acceptor (HBA). Assumptions are scored via a simulated annealing approach based on errors in the regression and complexity activity estimates. At the end of the optimization, the 10 unique best hypotheses displaying five characteristics points were kept: cost values, correlation coefficients, root mean square deviation (RMSD) values, pharmacophore characteristics and the maximum adjustment value of the 10 best-ranked hypotheses (Hypo1–Hypo10). These characteristics are listed in Table 4.The reliability of the PH4 models was then assessed using the calculated cost parameters ranging from 62.4 (Hypo1) to 122.1 (Hypo10). Their statistical data (costs, root mean square deviation RMSD, R^2) are listed in Table 6; 1.66≤ RMSD ≤ 3.32 and 0.88≤ R^2 ≤ 0.97. The PH4 hypo1 with the best RMSD and the highest R^2 was retained for further analysis; its regression equation pIC_{50}^{exp} = 0.93×pIC_{50}^{pre} + 0.47 (plot in Figure 6); n=15; R^2 = 0.97; R^2_{xv} = 0.94; F-test of 215.45; σ = 0.17; α > 98% with attest to the predictive capacity of the PH4 model. For this model, the fixed cost (39.49) is less than the zero cost (389.78) by a difference D = 350.29. This difference is a major indicator of the quality of PH4 predictability (D > 70 corresponds to an excellent chance or a probability greater than 90% that the model represents a true correlation **[42]**). Moreover, the configuration cost (11.82 for all assumptions) is well below 17 confirms this pharmacophore as reasonable **[48].** The link between the 98% significance and the number of 49 scrambled runs of each hypothesis is based on the formula S = [1 − (1 + X)/Y] × 100. with X the total number of hypotheses having a total cost lower than the starting assumption (Hypo 1) and Y the total number of HypoGen runs (initial + random draws): X = 0 and Y = (1 + 49). So 98% = {1 − [(1 + 0)/(49 + 1)]} × 100. From all the above. The first hypothesis (Hypo1) was retained. We have designed a virtual library taking into account the active centers indicated by the PH4 at the level of the substitution zone (figure5.A) namely a hydrophobic aromatic ring and an aliphatic hydrophobic group. This library has been screened by PH4 in order to obtain new. More potent analogs that can inhibit InhA from *Mycobacterium tuberculosis*.

3.6 Generation of virtual library and it's *in silico* screening

In silico screening of a virtual library (combinatorial) can lead to the identification of hits as demonstrated in our previous work on inhibitor design **[24,31,33,34,49]**.

3.6.1 Virtual Library

A virtual library (VL) was generated through substitutions at the R position of the thiadiazole scaffold. To do this, three rings were selected (thiophene, furan and pyridine) then underwent substitutions at their X, Y and Z position by aliphatic groups (Table 5). This first library obtained has 3x10x20x13 = 7800 analogues. To design a more targeted library of reduced size and increased content of drug-like molecules, we introduced a set of filters and penalties such as Lipinski's rule of fives **[50]** which allowed selecting a smaller number of TDZs that can be screened in silico. This focus reduced the size of the first library to 990.

3.6.2 *In silico* screening of library TDZs

The targeted library of 990 analogs was then screened for mole-cular structures matching the 3D-QSAR PH4 pharmacophore model of Hypo1. 253 TDZs mapped to at least 2 pharmacophoric features including 58 to at least 3 PH4 features. These best-fit analogs (PH4 hits) then underwent complexation QSAR model screening. The GFE calculation of InhA-TDZx complex formation,

Table 4: Parameters of 10 generated PH4 pharmacophoric hypotheses for the InhA inhibitor after the CatScramble validation procedure (49 scrambled runs for each hypothesis at the selected confidence level of 98%).

Hypothesis	RMSD [a]	R^2 [b]	Total Costs [c]	Difference [d]	Closest Random [e]	Features [f]
Hypo1	1.66	0.97	62.4	327.4	58.2	HBA HBD HYD HYD_Ar HYD_Al
Hypo2	2.54	0.93	89.4	300.4	84.6	HBA HBD HYD HYD_Ar HYD_Al
Hypo3	3.07	0.90	110.2	279.6	87.7	HBA HBD HYD HYD_Ar HYD_Al
Hypo4	3.16	0.89	114.4	275.4	90.2	HBA HBD HYD HYD_Ar HYD_Al
Hypo5	3.17	0.89	115.1	274.7	91.1	HBA HBD HYD HYD_Ar HYD_Al
Hypo6	3.25	0.88	119.0	270.8	91.8	HBA HBD HYD HYD_Ar HYD_Al
Hypo7	3.26	0.88	119.2	270.6	92.2	HBA HBD HYD HYD_Ar HYD_Al
Hypo8	3.26	0.88	119.5	270.3	92.7	HBA HBD HYD HYD_Ar HYD_Al
Hypo9	3.32	0.88	122.1	267.8	93.7	HBA HBD HYD HYD_Ar HYD_Al
Hypo10	3.32	0.88	122.8	267.8	93.7	HBA HBD HYD HYD_Ar HYD_Al

[a] root mean square deviation; [b] squared correlation coefficient; [c] overall cost parameter of the PH4 pharmacophore; [d] cost difference between Null cost and total cost of this hypothesis; [e] lowest cost of 49 scrambled runs at a selected level of confidence of 98%. Fixed Cost = 39.49 with RMSD = 0, Null Cost = 389.78 with RMSD = 6.96 and Configuration cost = 11.82. [f] HBA (hydrogen-bond acceptor); HYD (hydrophobic); HYD-Al (hydrophobic aliphatic); HYD-Ar (hydrophobic aromatic).

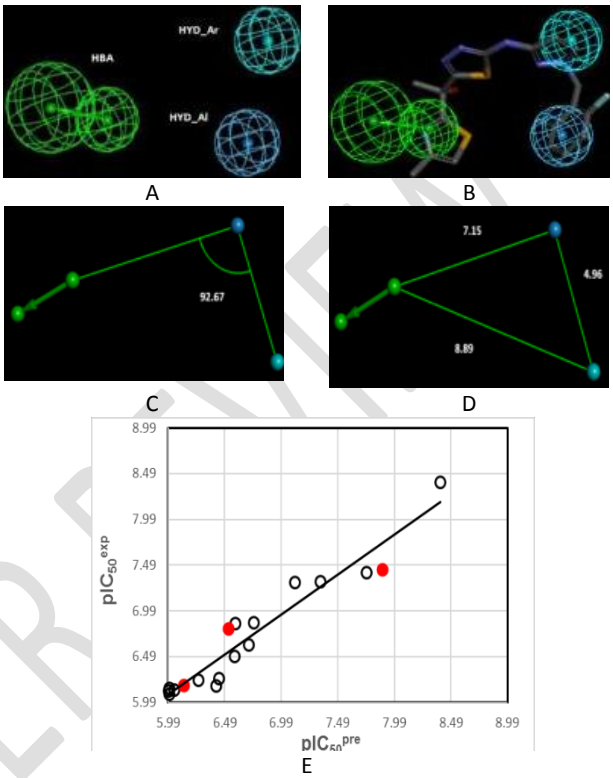

Figure 5: Features of the best PH4 model (Hypo1) of InhA inhibitors generated by the 3D-QSAR pharmacophore module: (**A**) Coordinates of the centers. (**B**) Mapping of Hypo1 with TDZ1 (the most potent TDZ molecule of the training set). (**C**) Angles (In degree) between the centers. (**D**) Distances in Å between the centers of the pharmaco-phoric features. Color code of features: blue (hydrophobic aliphatic); green (hydrogen bond acceptor); cyan (hydrophobic aromatic). (**E**) Plot of linear correlation of experimental vs predicted inhibitory activity. The validation set data points are shown in red color.

its components and the predicted half-maximal inhibition concentrations IC_{50}^{pre} calculated from correlation equation (B) (Table 3) is listed in Table 6.

Table 5: R Group (fragments. building blocks. substituents) used in the design of the initial thiadiazole diversity virtual combinatorial library.

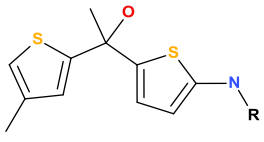

R	A	B	C
	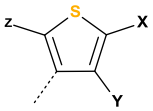	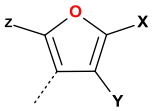	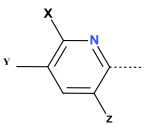
	THIOPHENE	FURANE	PYRIDINE

X1	X2	X3	X4	X5	X6	X7

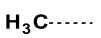	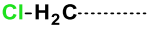	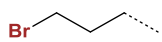	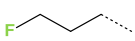	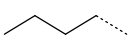		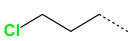
methyl	chloromethyl	1-bromopropyl	1-fluoropropyl	butyl	fluoromethyl	1-chloropropyl
X8	**X9**	**X10**	**Y1**	**Y2**	**Y3**	**Y4**
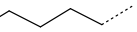	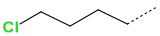	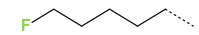	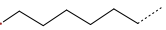	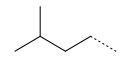	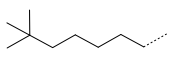	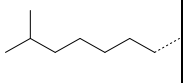
1-fluorobutyl	1-chlorobutyl	1-fluoropentyl	1-bromohexyl	2-methylbutyl	2.2-dimethylheptyl	2-methylheptyl
Y5	**Y6**	**Y7**	**Y8**	**Y9**	**Y10**	**Y11**
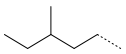	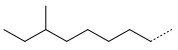		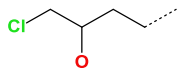	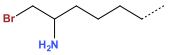	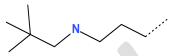	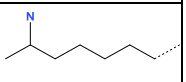
3-methylpentyl	3-methyloctyl	2-chloro-3-ethylpentyl	1-chlorobutyl-2-ol	1-bromohexyl-2-amine	neopentyl-N- propyl-1-amine	heptyl-2-amine
Y12	**Y13**	**Y14**	**Y15**	**Y16**	**Y17**	**Y18**
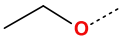	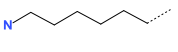		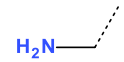	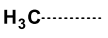		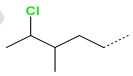
Oxyl-ethane	hexyl-1-amine	1-chloro-1-fluoro-methyl	methylamine	methyl	formylamide	2-chloro-3-methylpentyl
Y19	**Y20**	**Z1**	**Z2**	**Z3**	**Z4**	**Z5**
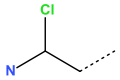	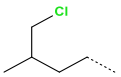	H	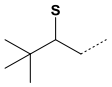	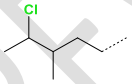	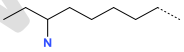	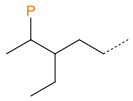
1-chloroethyl-1-amine	1-chloro-2-methylbutyl	hydrogen	3.3-dimethylbutyl-2-thiol	2-chloro-3-methylpentyl	octyl-3-amine	1-chlorobutyl-2-ol
Z6	**Z7**	**Z8**	**Z9**	**Z10**	**Z11**	**Z12**
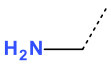	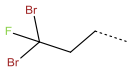	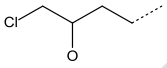	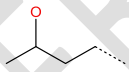	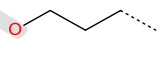	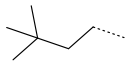	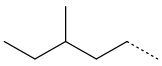
methylamine	1.1-dibromo-1-fluoropropyl	1-chlorobutyl-2-ol	butyl-2-ol	propyl-1-ol	2.2-dimethylbutyl	3-methylpentyl
Z13						
ethylamine						

Table 6: Relative GFE and their components for the top scoring 58 virtual TDZ analogs. The analogs numbering concatenates the index of each substituent R with the substituent numbers taken from Table 5.

N°	TDZ Analogs	M_w[a]	$\Delta\Delta_{HMM}$[b]	$\Delta\Delta G_{sol}$[c]	$\Delta\Delta TS_{vib}$[d]	$\Delta\Delta G_{com}$[e]	IC_{50}^{pre}[f] [nM]
Ref.	TDZ1	434	0	0	0	0	4[g]
1	B-X8-Y20-Z1	487	-7.24	0.56	1.82	-8.50	0.1
2	B-X5-Y15-Z1	394	0.19	-5.54	2.23	-7.58	0.1
3	B-X2-Y7-Z1	489	-7.42	-0.18	-0.41	-7.19	0.1
4	B-X2-Y15-Z1	386	3.30	-11.12	-0.90	-6.92	0.1
5	A-X1-Y12-Z11	467	0.77	0.36	7.83	-6.70	0.1
6	B-X10-Y16-Z1	411	-4.41	0.02	1.90	-6.29	0.2
7	C-X6-Y12-Z12	480	4.26	-6.93	3.48	-6.15	0.2
8	B-X4-Y14-Z1	435	-2.61	-4.19	-0.94	-5.86	0.2
9	C-X6-Y16-Z12	450	2.86	-5.09	3.56	-5.78	0.2
10	B-X9-Y19-Z1	476	-2.96	-2.50	0.03	-5.49	0.2
11	B-X8-Y14-Z1	449	-8.62	2.23	-1.07	-5.32	0.3
12	B-X6-Y12-Z11	469	6.93	-4.15	7.89	-5.11	0.3
13	A-X4-Y20-Z1	489	3.89	-7.28	1.07	-4.46	0.4
14	C-X1-Y20-Z1	438	0.23	-0.72	2.54	-3.03	1
15	A-X1-Y12-Z2	499	1.62	1.02	5.64	-3.00	1.1
16	B-X4-Y5-Z1	487	1.85	-1.39	2.88	-2.42	1.5
17	A-X6-Y16-Z11	455	1.63	1.55	5.43	-2.25	1.7
18	C-X2-Y20-Z1	472	3.05	-3.07	1.80	-1.82	2.3
19	C-X7-Y13-Z1	495	13.84	-8.66	6.89	-1.71	2.4
20	B-X7-Y16-Z1	399	-2.13	2.11	1.26	-1.28	3.2
21	C-X1-Y18-Z1	452	3.31	-2.00	2.12	-0.81	4.4
22	C-X4-Y5-Z6	493	15.22	-9.77	6.13	-0.68	4.7
23	B-X1-Y20-Z1	427	0.00	0.08	0.68	-0.60	5.0
24	B-X5-Y16-Z1	379	-1.59	2.16	1.02	-0.45	5.5
25	A-X6-Y16-Z2	487	2.57	0.63	3.23	-0.04	7.3
26	B-X4-Y18-Z1	487	2.57	0.33	2.90	0.00	7.5
27	B-X1-Y12-Z12	451	11.65	-7.58	4.04	0.02	7.6

N°	TDZ Analogs	M_w[a]	$\Delta\Delta_{HMM}$[b]	$\Delta\Delta G_{sol}$[c]	$\Delta\Delta TS_{vib}$[d]	$\Delta\Delta G_{com}$[e]	IC_{50}^{pre}[f] [nM]
28	C-X1-Y5-Z6	481	8.69	-5.60	3.05	0.04	7.6
29	B-X2-Y20-Z1	461	-2.75	1.10	-1.71	0.06	7.8
30	B-X1-Y20-Z6	456	0.84	0.29	0.81	0.32	9.3
31	C-X1-Y14-Z12	484	12.46	-8.89	2.94	0.64	11.4
32	B-X5-Y8-Z1	471	4.61	-0.86	2.94	0.82	12.8
33	A-X2-Y12-Z10	475	-1.00	2.17	0.06	1.10	15.5
34	A-X8-Y12-Z1	443	1.82	0.30	0.31	1.81	24.6
35	A-X5-Y12-Z1	425	2.74	0.44	1.17	2.01	28.1
36	C-X2-Y2-Z1	438	12.41	-8.13	1.84	2.45	37.6
37	C-X7-Y2-Z1	466	18.41	-11.05	4.80	2.56	40.5
38	A-X1-Y20-Z6	472	4.58	-0.39	1.50	2.69	44.1
39	A-X4-Y13-Z1	484	-6.88	14.41	4.69	2.83	48.5
40	B-X2-Y16-Z12	455	7.63	-0.07	3.82	3.74	49
41	A-X1-Y13-Z1	438	11.01	-7.23	0.72	3.07	56.7
42	A-X10-Y12-Z1	457	4.08	1.99	2.23	3.84	94.7
43	A-X6-Y20-Z6	490	3.49	1.50	0.90	4.09	111
44	C-X1-Y15-Z12	481	16.05	-8.24	3.15	4.66	163
45	A-X1-Y12-Z1	383	5.64	0.97	1.48	5.12	221
46	A-X6-Y12-Z1	401	3.58	1.22	-0.61	5.41	268
47	A-X1-Y11-Z1	452	10.77	0.17	5.43	5.51	285
48	A-X1-Y12-Z9	455	3.02	5.02	2.31	5.72	328
49	B-X1-Y20-Z9	499	5.60	7.47	7.13	5.94	379
50	B-X1-Y15-Z12	436	12.20	0.44	6.57	6.06	411
51	A-X10-Y14-Z1	479	0.07	4.04	-2.16	6.28	473
52	A-X1-Y12-Z10	441	7.74	1.17	2.29	6.62	596
53	C-X2-Y2-Z6	467	18.09	-8.11	2.24	7.74	1244
54	A-X1-Y12-Z8	489	7.26	0.81	-0.57	8.64	2266
55	C-X2-Y5-Z13	495	20.09	-6.47	4.62	8.99	2859
56	C-X2-Y7-Z6	495	20.53	-7.26	3.82	9.46	3889
57	A-X2-Y20-Z1	477	8.40	0.14	-1.03	9.56	4168
58	B-X6-Y20-Z1	445	3.63	1.63	-4.93	10.19	6324

[a] M_w is the molar mass of the inhibitor; [b] $\Delta\Delta H_{MM}$ is the relative enthalpy contribution to the GFE change of InhA-TDZ upon formation of the ΔΔGcom complex (for details. see footnote to Table 2); [c] $\Delta\Delta G_{sol}$ is the solvation GFE contribution relative to $\Delta\Delta G_{com}$; [d]$\Delta\Delta TS_{vib}$ is the relative (vibrational) entropic contribution to $\Delta\Delta G_{com}$; [e]$\Delta\Delta G_{com}$ is the relative Gibbs free energy change related to the formation of the InhA-TDZ enzyme-inhibitor complex $\Delta\Delta G_{com} = \Delta\Delta H_{MM} + \Delta\Delta G_{sol} - \Delta\Delta TS_{vib}$; [f]$IC_{50}^{pre}$ is the predicted inhibitory potency towards InhA calculated from $\Delta\Delta G_{com}$ using the correlation equation (B), Table 3; [g]IC_{50}^{exp} is given for the reference inhibitor TDZ1 instead of IC_{50}^{pre}.

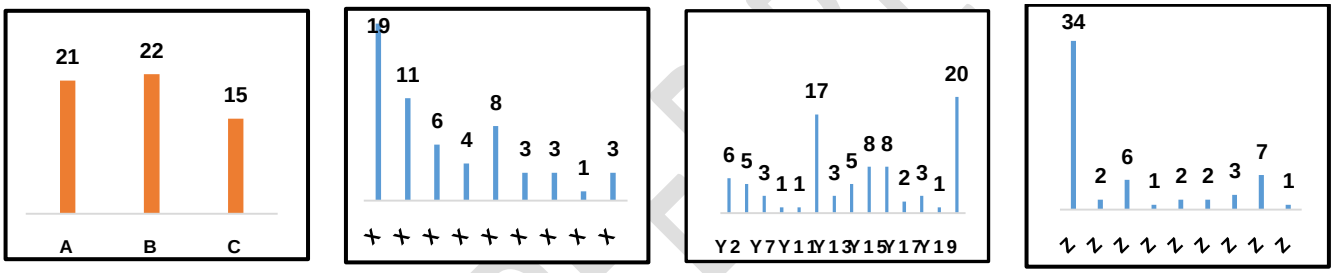

(A) (B) (C) (D)

Figure 6: Histograms of occurrence frequency of individual R groups in the 58 best selected analogs

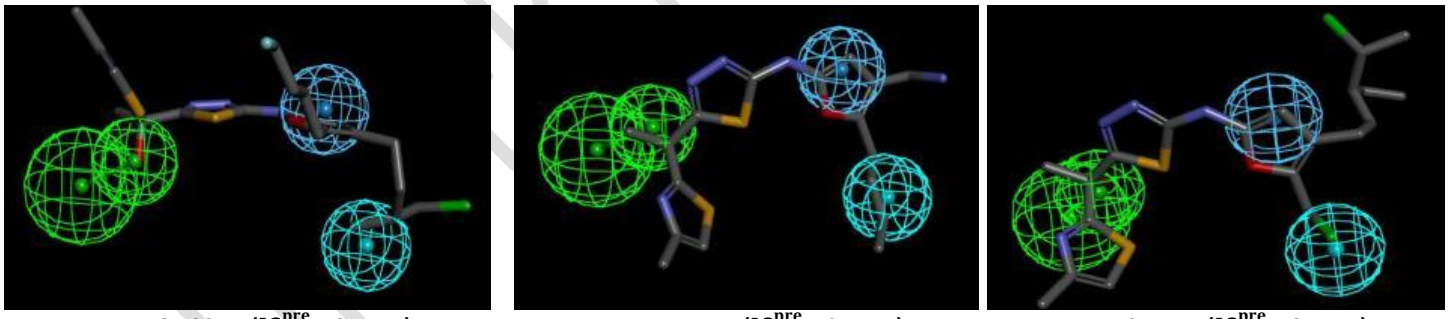

TDZ-B-X8-Y20-Z1 (IC_{50}^{pre} = 0.1 nM) **TDZ-B-X5-Y15-Z1 (IC_{50}^{pre} = 0.1 nM)** **TDZ-B-X2-Y7-Z1 (IC_{50}^{pre} = 0.1 nM)**

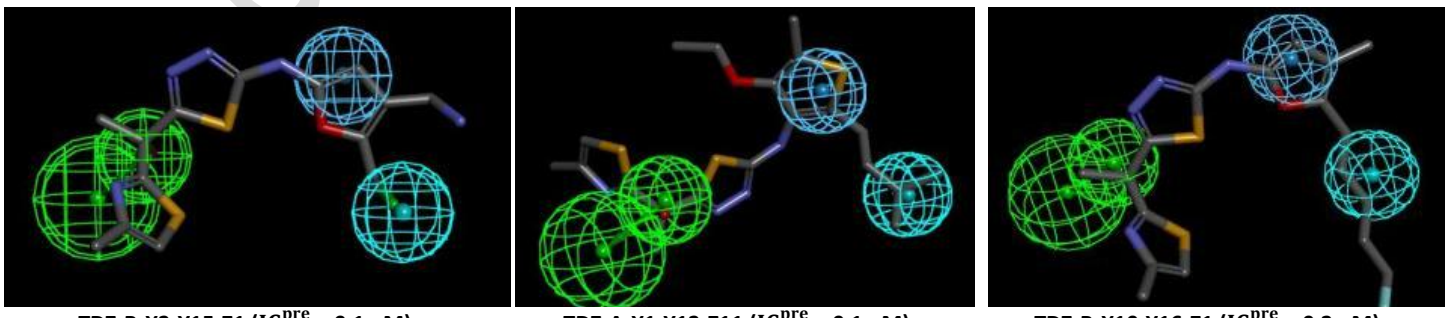

TDZ-B-X2-Y15-Z1 (IC_{50}^{pre} = 0.1 nM) **TDZ-A-X1-Y12-Z11 (IC_{50}^{pre} = 0.1 nM)** **TDZ-B-X10-Y16-Z1 (IC_{50}^{pre} = 0.2 nM)**

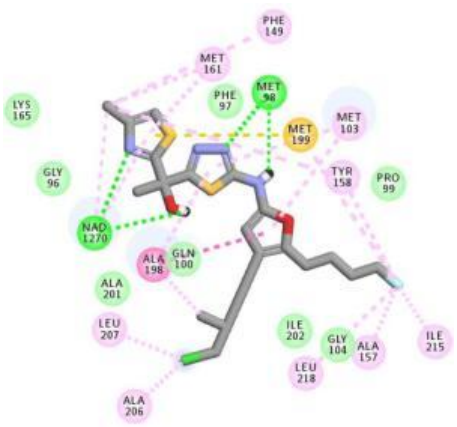

TDZ-B-X8-Y20-Z1 (IC_{50}^{pre} = 0.1 nM)

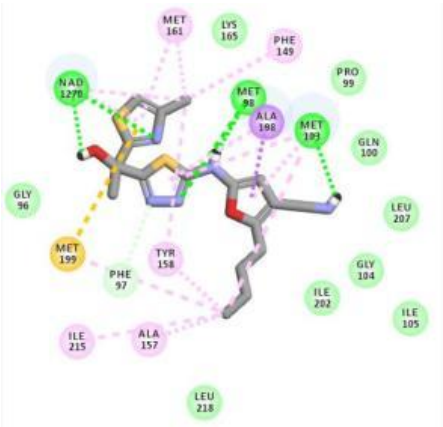

TDZ-B-X5-Y15-Z1 (IC_{50}^{pre} = 0.1 nM)

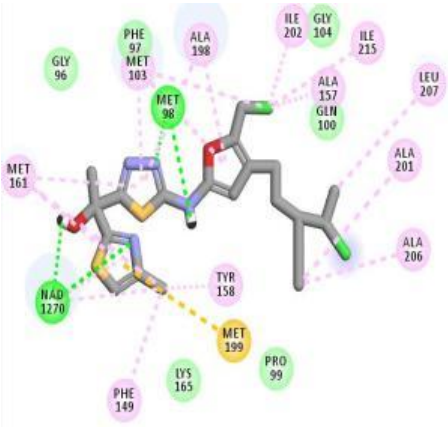

TDZ-B-X2-Y7-Z1 (IC_{50}^{pre} = 0.1 nM)

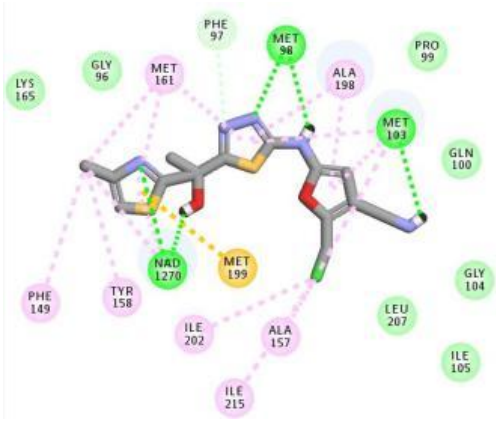

TDZ-B-X2-Y15-Z1 (IC_{50}^{pre} = 0.1 nM)

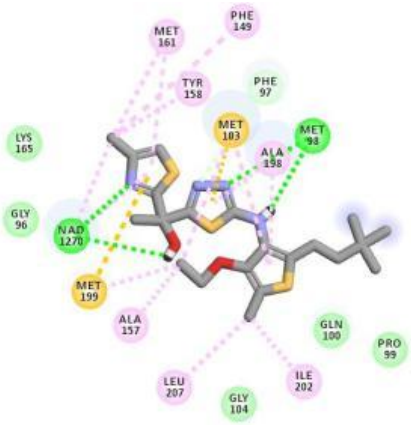

TDZ-A-X1-Y12-Z11 (IC_{50}^{pre} = 0.1 nM)

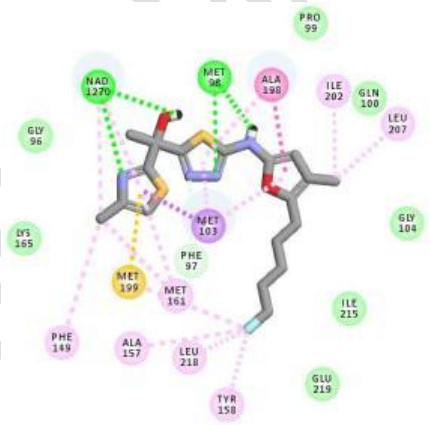

TDZ-B-X10-Y16-Z1 (IC_{50}^{pre} = 0.2 nM)

van der Waals

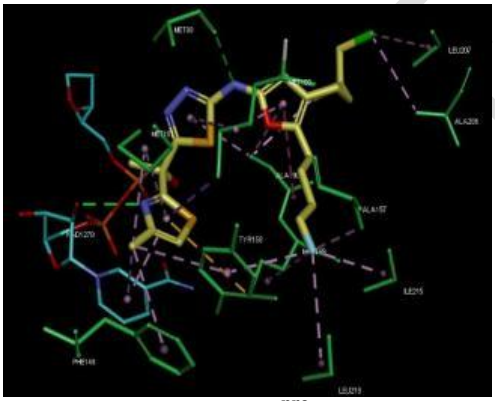

TDZ-B-X8-Y20-Z1 (IC_{50}^{pre} = 0.1 nM)

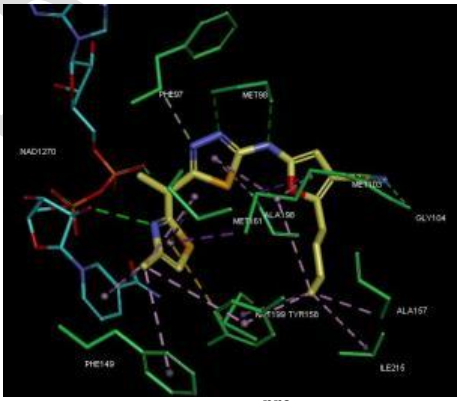

TDZ-B-X5-Y15-Z1 (IC_{50}^{pre} = 0.1 nM)

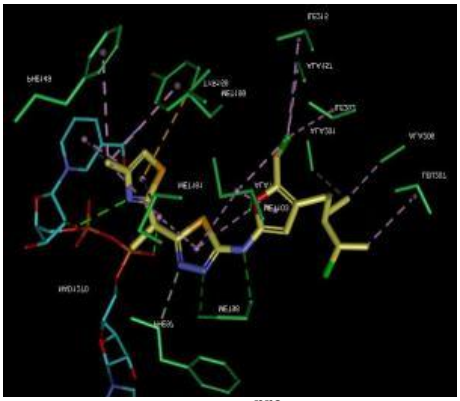

TDZ-B-X2-Y7-Z1 (IC_{50}^{pre} = 0.1 nM)

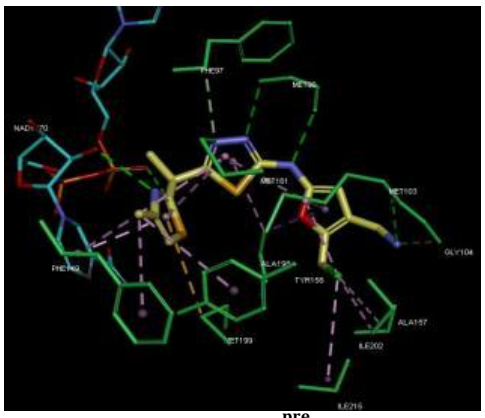

TDZ-B-X2-Y15-Z1 (IC_{50}^{pre} = 0.1 nM)

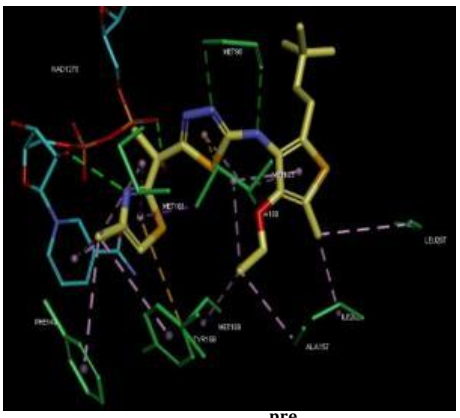

TDZ-A-X1-Y12-Z11 (IC_{50}^{pre} = 0.1 nM)

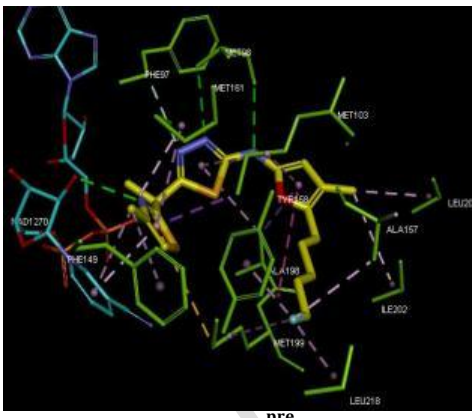

TDZ-B-X10-Y16-Z1 (IC_{50}^{pre} = 0.2 nM)

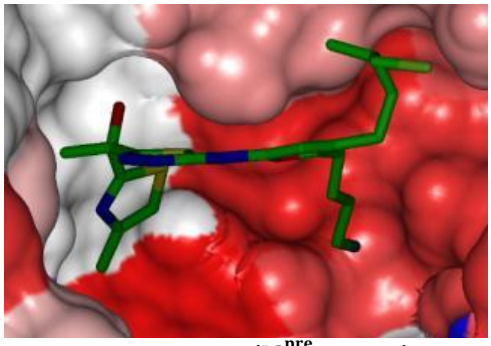

TDZ-B-X8-Y20-Z1 (IC_{50}^{pre} = 0.1nM)

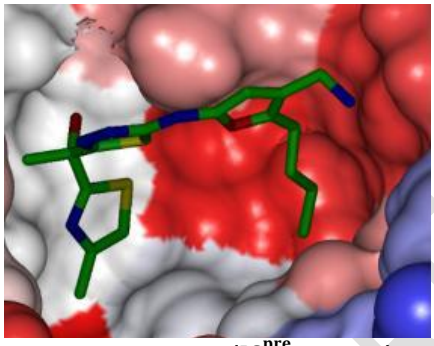

TDZ-B-X5-Y15-Z1 (IC_{50}^{pre} = 0.1 nM)

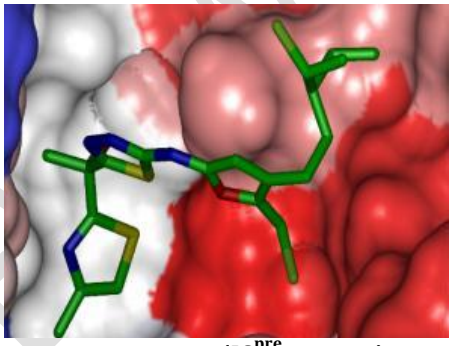

TDZ-B-X2-Y7-Z1 (IC_{50}^{pre} = 0.1 nM)

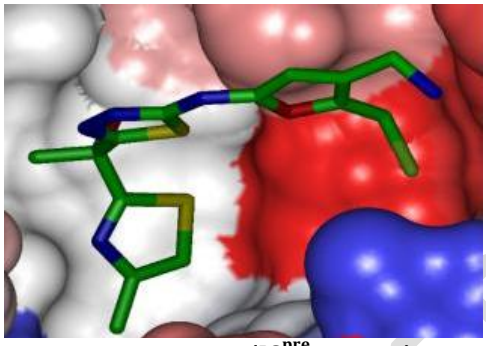

TDZ-B-X2-Y15-Z1 (IC_{50}^{pre} = 0.1 nM)

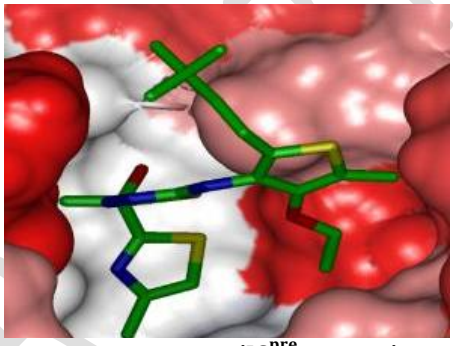

TDZ-A-X1-Y12-Z11 (IC_{50}^{pre} = 0.1 nM)

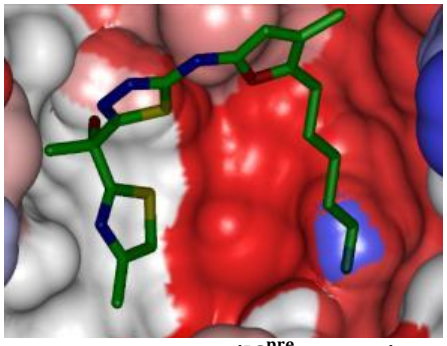

TDZ-B-X10-Y16-Z1 (IC_{50}^{pre} = 0.2 nM)

Figure 7: Mapping of analogs to InhA inhibition pharmacophore: TDZ-B-X8-Y20-Z1, TDZ-B-X5-Y15-Z1, TDZ-B-X2-Y7-Z1, TDZ-B-X2-Y15-Z1, TDZ-A-X1-Y12-Z11, TDZ-B-X10-Y16-Z1. 2D schematic interaction diagram of the analogs TDZ-B-X8-Y20-Z1; TDZ-B-X5-Y15-Z1, TDZ-B-X2-Y7-Z1, TDZ-B-X2-Y15-Z1, TDZ-A-X1-Y12-Z11, TDZ-B-X10-Y16-Z1. Connolly surface of InhA active site withanalogs TDZ-B-X8-Y20-Z1, TDZ-B-X5-Y15-Z1, TDZ-B-X2-Y7-Z1, TDZ-B-X2-Y15-Z1, TDZ-A-X1-Y12-Z11, TDZ-B-X10-Y16-Z1. The surface of the binding site is colored according to the hydrophobicity of the residues: red - hydrophobic, blue - hydrophilic and white – intermediate

3.7 Pharmacokinetic profile of new analogs TDZ

ADME-related properties (absorption. distribution. metabolism and excretion) were estimated for the designed analogs as well as for some selected reference anti-TB drugs. The best engineered TDZ derivatives with poor oral bioavailability due to low water solubility and rapid phase II metabolism should be disregarded for possible use as anti-tuberculosis drugs. All ADME-related properties shown in Table 7 such as octanol-water partition coefficient, aqueous solubility, blood-brain partition coefficient, Caco-2 cell permeability, serum protein binding, number of probable metabolic reactionsand 18 other descriptors of the new analogues were calculated by the QikProp program **[51]**based on the Jorgensen method **[52,53]**. Experimental data for over 710 compounds including approximately 500 drugs and related heterocyclic were used to generate regression equations correlating the experimental and calculated descriptorsresulting in an accurate prediction of the pharmacokinetic properties of drug-like molecules. The predicted oral bioavailability for the new TDZ analogs ranges from (71-100) % and is significantly higher than that of triclosan where the best active derivative has unfavorable oral bioavailability. Since a value above 80% is considered good, our TDZ analogs show good human oral absorption from the gastrointestinal tract (HOA). Drug-like (#stars), the number of property descriptors that fall outside the range of optimal values determined for 95% of known drugs out of 24 selected descriptors calculated by QikProp was used as an additional selection criterion for ADME-related compounds. The values of the best designed TDZs are compared with those calculated for drugs used for the treatment of tuberculosis or in clinical trials (Table 7). Our best-designed analogues all show #stars equal to 0 or 1, which means that the optimal range of values for any of the addiction descriptors has not been violated. Thus our six best designed TDZ analogs have a much more interesting pharmacokinetic profile in the development of InhA inhibitors of *Mycobacterium tuberculosis*.

4. DISCUSSION

To better understand the inhibitory power of our designed analogs, visual analysis shows us a better filling of the hydrophobic pocket [**4545**] of our active site by slightly larger fragments capped by the furan and thiophene ring. Indeed, the fragments X1 (methyl), X2 (chloromethyl), X5 (butyl), X8 (fluorobutyl), X10 (fluoropentyl), Y7 (2-chloro-3-ethylpentyl), Y12 (oxyl-ethane), Y15 (methylamine), Y16 (methyl), Y20 (1-chloro-2-methylbutyl) and Z11 (2.2-dimethylbutyl) interacted significantly with the pocket residues. The most active analogues exemplified by TDZ-B-X8-Y20-Z1 (Figure 7) with a predicted inhibitory potency of IC_{50}^{pre} =0.1 nM, i.e. 40 times more active than our best active training set ligand TDZ1 (IC_{50}^{pre} = 4 nM), due toVdW interactions with Pro99, Gln100, Gly104, Ala201 and Ile202 whileits furan ring establishes a Pi-stacked amide-like hydrophobic bond with Ala198 and a Pi-alkyl interaction with Met103. Fluorobutyl through fluorine establishes alkyl interactions with Tyr158, Ala157, Ile215 and Leu218 while there are alkyl interactions between the methyl of 1-chloro-2-methylebutyl with Ala198 on the one hand; and on the other hand between chlorine and Ala 206 and Leu207. Similarly, a hydrogen bond (HB) was established between the NH of the methylamine fragment and the "O" of the carbonyl group of Met103 and alkyl interactions between the butyl with Met103, Ala157, Tyr158 and Ile215. The individual contribution in interaction energy of the residues (figure 8) confirms our results. For example in the case of our most active analogue TDZ-B-Y20-X8-Z1, the contributions at the level of most active site residues strongly increased in comparison to the those with our most active training set TDZ1 as shown in figure 8. Interactions identified through RX crystallography analysis from the starting structure [**28**] are conserved and improved for some of them with relevant R-group substitutions.

We notice that the interaction of our analog doubled with Gln100, was multiplied by 11 with Ala206 and by approximately 3 with Leu218. These strong interactions of our analog with these residues therefore contributed to its stabilization in the active site of InhA. All of the above substantiates the inhibitory power of our six best engineered analogs: TDZ-B-X8-Y20-Z1 (IC_{50}^{pre} =0.1 nM),TDZ-B-X5-Y15-Z1(IC_{50}^{pre} =0.1 nM),TDZ-B-X2-Y7-Z1(IC_{50}^{pre} =0.1 nM),TDZ-B-X2-Y15-Z1 (IC_{50}^{pre} =0.1 nM), TDZ-A-X1-Y12-Z11 (IC_{50}^{pre} =0.1 nM), TDZ-B-X10-Y16-Z1 (IC_{50}^{pre} =0.2 nM).

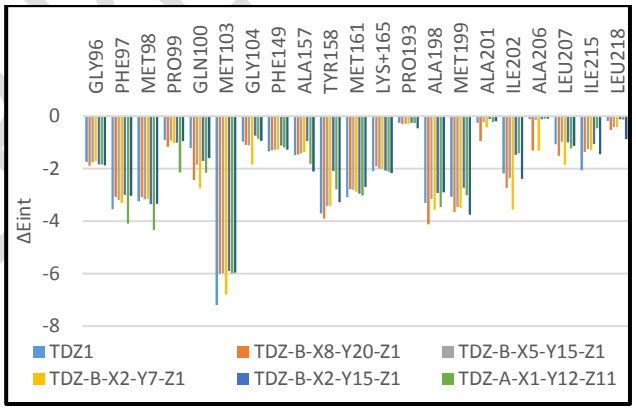

Figure 8: Interaction energy per residue with the most active ligand of the TDZ1 test set (IC_{50}^{exp} = 4 nM) and the six best analogues obtained: TDZ-B-X8-Y20-Z1 (IC_{50}^{pre} = 0.1 nM), TDZ-B-X5-Y15-Z1 (IC_{50}^{pre} = 0.1 nM), TDZ-B-X2-Y7-Z1 (IC_{50}^{pre} = 1 nM), TDZ-B-X2-Y15-Z1 (IC_{50}^{pre} . = 0.1 nM), TDZ-A-X1-Y12-Z11 (IC_{50}^{pre} = 0.1 nM), TDZ-B-X10-Y16-Z1 (IC_{50}^{pre} = 0.2 nM).

5. CONCLUSION

InhA is a promising target in the development and research of new anti-TB drugs due to its role in the final step of mycolic acid synthesis [9]. The crystallographic structure of the InhA-TDZ1 (4BQP) complex and the structural properties of the thiadiazole derivatives identified by Roman Sink *et al.***[28]** as a potential antituberculosis agent and whose target is InhA enabled us to develop a QSAR complexation model capable of explaining more than 92% of the variation in the experimental inhibitory activity of thiadiazole derivatives by the Gibbs free energy of formation of the InhA-TDZx complex. Following this QSAR model, we obtained a 3D-QSAR PH4 pharmacophore model using a training set of 15 TDZs and a validation set of 3 TDZs with known inhibitory activities [**28**]. The visual analysis and calculation of the interactions between InhA and TDZs in the active site of the

enzyme guided us in the design of a virtual combinatorial library of new TDZ analogs with a substitution on the TDZ scaffold at the position R. The library thus obtained was first focused according to Lipinski's rule of five and then screened by the pharmacophore. This allowed us to retain 58 best virtual hits which were subjected to the calculation of the inhibitory predicted potency by the QSAR complexation model. The six best analogs achieved the expected activities in the subnanomolar concentration range: TDZ-B-X8-Y20-Z1, TDZ-B-X5-Y15-Z1, TDZ-B-X2-Y7-Z1, TDZ-B-X2-Y15-Z1, TDZ-A-X1-Y12-Z11 all with a predicted potency of 0.1 nM (IC_{50}^{pre} = 0.1 nM) and TDZ-B-X10-Y16-Z1 (IC_{50}^{pre} = 0.2 nM). In addition to their activities these molecules present a favorable predicted pharmacokinetic profile and deserve to be synthesized and biologically evaluated.

CONSENT

It is not applicable.

ETHICAL APPROVAL

It is not applicable.

Table 7. ADME-related properties of the best designed TDZ analogs and known antituberculotic agents either in clinical use or currently undergoing clinical testing computed by QikProp **[54]**

	#star[b]	MW[c] [g.mol^{-1}]	Smol [Å^2]	Smol.hfoe [Å^2]	Vmol [Å^3]	RotBg	HBdonh	HBacci	logPo/wj	logSwatk	logKHSAl	logBB/Bcacom	IP cacon [nm.s^{-1}]	#metabo	IC$_{50}$ [nM]	HOAq	%HOAr
TDZ-B-X8-Y20-Z1	1	487	773	440	1453	11	2	5	5.9	-7.1	1.0	-0.9	837	7	0.1	1	100
TDZ	1	394	687	380	124	10	4	6	2.5	-3.	0.2	-1.	60	9	0.1	2	73
-B-X5-Y15-Z1						0				5		3					
TDZ-B-X2-Y7-Z1	1	489	771	417	1418	10	2	5	5.7	-7.3	1.0	-0.9	825	7	0.1	1	100
TDZ-B-X2-Y15-Z1	1	386	618	249	1096	7	4	6	1.9	-3.1	0.0	-0.8	71	9	0.1	2	71
TDZ-A-X1-Y12-Z11	1	467	764	549	1437	10	2	6	5.5	-6.7	1.0	-0.9	1298	8	0.1	1	100
TDZ-B-X10-Y16-Z1	0	411	713	411	1286	9	2	5	4.6	-6.1	0.6	-0.9	860	7	0.2	3	100

	1	137.1	314	0.0	480*	2	-3	4.5	−0.7	0	−0.8	−0.8	267.5	2		2	67
	4	123.1*	300	0.0	443*	1	2	5	−0.6	−0.5	−0.8	−0.7	298.4	4		2	67
	2	204.3	476	395.8	806	11	4	64.4	−0.2	0.6	−0.8	0.0	107.8	4		2	62
Pyrazinamide	10	823.0*	1090*	850.0*	2300*	25*	6	20.3*	3.0	−3.1	−0.3	−2.7	38.2	11*		1	34
Ciprofloxacin	0	375.4	598	355.7	1093	2	1	6.8	0.5	−4.0	0	−0.6	17.0	1		2	52
Moxifloxacin	0	401.4	642	395.6	1168	2	1	6.8	1.0	−4.7	0.2	−0.6	20.9	1		2	56
	10	877.0*	1025*	844.9*	2333*	24*	6	20.9*	3.6	−2.2	−0.2	−1.5	224.0	13*		1	51

	4	555.5	787	213.7	1532	9	1	3.8	7.6*	−6.9	1.7	0.4	1562.2	5		1	100
	2	534.5	796	284.4	1470	7	0	6.0	5.8	−7.6	1.0	−1.0	590.9	2		1	85
	0	337.4	555	337.2	996	2	1	8.7	0.6	−2.0	−0.7	−0.5	507.0	2		3	79
	1	353.4	594	330.6	1047	2	1	7.5	1.3	−3.4	−0.4	−0.4	449.3	0		3	82
	1	361.4	581	337.0	1044	1	0	7.3	−0.4	−2.8	−0.5	−0.4	25.9	1		2	50
	14	585.6	739	350.3	1500	22*	17*	26.9*	−7.9*	−0.2	−2.1	−3.5	0	14*		1	0
	10	484.5	656	258.9	1291	17*	15*	22.7*	−6.7*	2.0	−1.4	−3.1	0	12*		1	0
	0	299.3	487	259.1	880	8	3	7.2	1.0	−1.8	−0.7	−1.4	35.0	3		3	61

	2	365.4	561	164.6	1033	6	4.25	8.0	−2.5	−0.8	−1.1	−1.5	1.0	5		1	12
	0	199.2	397	184.6	630	4	2	6.5	−0.8	0.3	−1.3	−1.3	13.3	2		2	42

[a] designed TDZ analogs and known antituberculotic agents. Table 8; [b] drug likeness. number of property descriptors (24 out of the full list of 49 descriptors of QikProp. ver. 3.7. release 14) that fall outside of the range of values for 95% of known drugs; [c] molar mass in [g.mol^{-1}] (range for 95% of drugs: (130–725) g.mol^{-1}) [51]; [d] total solvent-accessible molecular surface in [Å^2] (probe radius 1.4 Å) (range for 95% of drugs: (300–1000) Å^2); [e] hydrophobic portion of the solvent-accessible molecular surface in [Å^2] (probe radius 1.4 Å) (range for 95% of drugs: (0–750) Å^2); [f] total volume of molecule enclosed by solvent-accessible molecular surface in [Å^3] (probe radius 1.4 Å) (range for 95% of drugs: (500–2000) Å^3); [g] number of non-trivial (not CX3) non-hindered (not alkene, amide, small ring) rotatable bonds (range for 95% of drugs: 0–15); [h] estimated number of hydrogen bonds that would be donated by the solute to water molecules in an aqueous solution. Values are averages taken over a number of configurations so they can assume non-integer values (range for 95% of drugs: 0.0–6.0); [i] estimated number of hydrogen bonds that would be accepted by the solute from water molecules in an aqueous solution. Values are averages taken over a number of configurations so they can assume non-integer values (range for 95% of drugs: 2.0–20.0); [j] logarithm of partitioning coefficient between n-octanol and water phases (range for 95% of drugs: −2 to 6.5); [k] logarithm of predicted aqueous solubility logS. S in [mol.dm^{-3}] is the concentration of the solute in a saturated solution that is in equilibrium with the crystalline solid (range for 95% of drugs: −6.0 to 0.5); [l] logarithm of predicted binding constant to human serum albumin (range for 95% of drugs: −1.5 to 1.5); [m] logarithm of predicted brain/blood partition coefficient (range for 95% of drugs: −3.0 to 1.2); [n] predicted apparent Caco-2 cell membrane permeability in Boehringer-Ingelheim scale in [nm s^{-1}] (range for 95% of drugs: < 25 poor. > 500 nm s^{-1} great); [o] number of likely metabolic reactions (range for 95% of drugs: 1–8); [p] predicted inhibition constants IC_{50}^{pre}. IC_{50}^{pre} was predicted from computed $\Delta\Delta G_{com}$ using the regression Equation B shown in Table 2; [q] human oral absorption (1 = low. 2 = medium. 3 = high); [r] percentage of human oral absorption in gastrointestinal tract (<25% = poor. >80% = high); * star in any column indicates that the property descriptor value of the compound falls outside the range of values for 95% of known drugs.

ABBREVIATIONS

2D	Two-dimensional
3D	Three-dimensional
ADME	Absorption, distribution, metabolism and excretion
E_{int}	MM enzyme–inhibitor interaction energy per residue
$\Delta\Delta G_{com}$	Relative complexation GFE
$\Delta\Delta H_{MM}$	Enthalpy Component of GFE
GFE	Gibbs free energy
$\Delta\Delta G_{sol}$	Relative solvation GFE
$\Delta\Delta TS_{vib}$	Relative entropic of GFE
HB	Hydrogen bond
HBA	Hydrogen bond Acceptor
HBD	Hydrogen bond Donor
H_{MM}	Enthalpy component of GFE
HOA	Human oral absorption
HYD	Hydrophobic
HYDA	Hydrophobic Aliphatic
IC_{50}	Half-maximal inhibitory concentration
IE	Interaction energy
InhA	2-trans enoyl-acyl carrier protein reductase
KatG	*Mycobacterium tuberculosis* catalase–peroxidase
MM	Molecular mechanics
MM-PB	Molecular mechanics–Poisson Boltzmann
M*tb*	Mycobacterium tuberculosis
NADH	nicotinamide adenine dinucleotide reduced
PDB	Protein Data Bank
PH4	Pharmacophore
QSAR	Quantitative structure–activity relationships
RMSD	Root-mean square deviation
SAR	Structure–activity relationships
TB	Tuberculosis
TS	Training set
VS	Validation set

REFERENCES

1 Hershkovitz I, Donoghue HD, Minnikin DE, May H, Lee OY, Feldman M, Galili E, Spigelman M, Rothschild BM, Bar-Gal GK. Tuberculosis origin: The Neolithic scenario. Tuberculosis (Edinb). Epub. 2015; 1-5. https://doi.org/10.1016/j.tube.2015.02.021

2 Sakula A. Robert Koch: centenary of the discovery of the tubercle bacillus. Thorax. 1982; 37(4): 246-51. https://doi.org/10.1136/thx.37.4.246

3 World Health Organization. Global tuberculosis report 2022. Geneva: 2022. Licence: CC BY-NC- SA 3.0 IGO.

4 Jain A, Mondal R. Extensively drug-resistant tuberculosis: current challenges and threats. FEMS Immunol. Med. Microbiol. 2008; 53: 145–50. https://doi.org/10.1111/j.1574-695X.2008.00400.x

5 Udwadia ZF, Amale RA, Ajbani KK, Rodrigues C. Totally drug-resistant tuberculosis in India. Clin. Infect. Dis. 2012; 54(4): 579–81. https://doi.org/10.1093/cid/ cir889

6 Koul A, Arnoult E, Lounis N, Guillemont J, Andries K. The challenge of new drug discovery for tuberculosis. Nature. 2011; 469(7331): 483–90. https://doi.org/10. 1038/nature09657

7 Palomino JC, Martin A. TMC207 becomes bedaquiline, a new anti-TB drug. Future Microbiol. 2013; 8(9): 1071–80. https://doi.org/10.2217/fmb.13.85

8 Fox GJ, Menzies D. A Review of the Evidence for Using Bedaquiline (TMC207) to Treat Multi-Drug Resistant Tuberculosis. Infect. Dis. Ther. 2013; 2(2): 123–44. https://doi.org/10.1007/s40121-013-0009-3

9 Gerusz V, Denis A, Faivre F, Bonvin Y, Oxoby M, Briet S, LeFralliec G, Oliveira C, Desroy N, Raymond C, Peltier L, Moreau F, Escaich S, Vongsouthi V, Floquet S, Drocourt E, Walton A, Prouvensier L, Saccomani M, Durant L, Genevard JM, Sam-Sambo V, Soulama-Mouze C. From Triclosan toward the clinic: discovery of nonbiocidal, potent FabI inhibitors for the treatment of resistant bacteria. J. Med. Chem. 2012; 55(22): 9914–28. https://doi.org/10.1021/jm301113w

10 Parikh S, Moynihan DP, Xiao GP, Tonge PJ. Roles of tyrosine 158 and lysine 165 in the catalytic mechanism of InhA, the enoyl-ACP reductase from *Mycobacterium tuberculosis*. Biochemistry. 1999; 38(41): 13623–34. https://doi.org/10.1021/bi990529c

11 Dessen A, Quemard A, Blanchard JS, Jacobs WR, Sacchettini JC. Crystal structure and function of the isoniazid target of Mycobacterium tuberculosis. Science. 1995; 267(5204): 1638–41. https://doi.org/ 10.1126/science.7886450

12 Rozwarski DA, Vilcheze C, Sugantino M, Bittman R, Sacchettini JC. Crystal structure of the Mycobacterium tuberculosis enoyl-ACP reductase, InhA, in complex with NAD (+) and a C16 fatty acyl substrate. J. Biol. Chem. 1999; 274(22): 15582–89. https://doi.org/10. 1074/jbc.274.22.15582

13 Rawat R, Whitty A, Tonge PJ. The isoniazid-NAD adduct is a slow, tight-binding inhibitor of InhA, the Mycobacterium tuberculosis enoyl reductase: adduct affinity and drug resistance. Proc. Natl. Acad. Sci. U. S. A. 2003; 100(24): 13881–86. https://doi.org/10.10 73/pnas.2235848100

14 Johnson K, King DS, Schultz PG. Studies on the Mechanism of Action of Isoniazid and Ethionamide in the Chemotherapy of Tuberculosis. J. Am. Chem. Soc. 1995; 117(17):5009–10. https://doi.org/10.1021/ ja00122a038

15 Basso LA, Zheng R, Blanchard JS. Kinetics of Inactivation of WT and C243S Mutant of Mycobacterium tuberculosis Enoyl Reductase by Activated Isoniazid. J. Am. Chem. Soc. 1996; 118(45): 11301–02. https://doi.org/10.1021/ja962035y

16 Magliozzo RS, Marcinkeviciene JA. Evidence for Isoniazid Oxidation by Oxyferrous Mycobacterial Catalase–Peroxidase. J. Am. Chem. Soc. 1996; 118(45): 11303–04. https://doi.org/10.1021/ja962047j

17 Zabinski RF, Blanchard JS. The Requirement for Manganese and Oxygen in the Isoniazid-Dependent Inactivation of Mycobacterium tuberculosis Enoyl Reductase. J. Am. Chem. Soc. 1997; 119(9): 2331–32. https://doi.org/10.1021/ja9639731

18 Young DB. Beating the bacillus. Curr. Biol. 1994; 4(4): 351–3. https://doi.org/10.1016/S0960-9822(00)00077-4

19 Blanchard JS. Molecular mechanisms of drug resistance in *Mycobacterium tuberculosis*. Annu. Rev. Biochem. 1996; 65(1): 215–39. https://doi.org/10.1146/annu rev.bi.65.070196.001243

20 Freundlich JS, Wang F, Vilcheze C, Gulten G, Langley R, Schiehser GA, Jacobus DR, Jacobs WR, Sacchettini JC. Triclosan derivatives: towards potent inhibitors of drug-sensitive and drug-resistant *Mycobacterium tuberculosis*. Chem Med Chem. 2009; 4(2): 241–48. https://doi.org/10.1002/cmdc.200800261

21 Parikh SL, Xiao GP, Tonge PJ. Inhibition of InhA, the enoyl reductase from Mycobacterium tuberculosis, by triclosan and isoniazid. Biochemistry. 2000; 39(26): 7645–50. https://doi.org/10.1021/bi0008940

22 Kuo MR, Morbidoni HR, Alland D, Sneddon SF, Gourlie BB, Staveski MM, Leonard M, Gregory JS, Janjigian AD, Yee C, Musser JM, Kreiswirth B, Iwamoto H, Perozzo R, Jacobs WR, Sacchettini JC, Fidock DA. Targeting tuberculosis and malaria through inhibition of enoyl reductase. J. Biol. Chem. 2003; 278(23): 20851–59. https://doi.org/10.1074/jbc.M211968200

23 Sivaraman S, Sullivan TJ, Johnson F, Novichenok P, Cui GL, Simmerling C, Tonge PJ. Inhibition of the bacterial enoyl reductase FabI by triclosan: A struc-ture–reactivity analysis of FabI inhibition by triclosan analogues. J. Med. Chem. 2004; 47(3): 509–18. https://doi.org/10.1021/jm030182i

24 Kouassi A, Kone M, Keita M, Esmel A, Megnassan E, N'Guessan Y, Frecer V, Miertus S. Computer- Aided Design of Orally Bioavailable Pyrrolidine Carboxamide Inhibitors of Enoyl-Acyl Carrier Protein Reductase of Mycobacterium tuberculosis with Favorable Pharma-cokinetic Profiles. Int. J. Mol. Sci. 2015; 16(12): 29744–71. https://doi.org/10.3390/ijms161226196

25 Kouman KC, Keita M, Kre N'Guessan R, Owono Owono LC, Megnassan E, Frecer V, Miertus S. Structure-Based Design and in Silico Screening of Virtual Combinatorial Library of Benzamides Inhibiting 2-trans Enoyl-Acyl Carrier Protein Reductase of Mycobacterium tuberculosis with Favorable Predicted Pharmaco-kinetic Profiles. Int. J. Mol. Sci. 2019; 20(19):4730-61 https://doi.org/10.3390/ijms20194730

26 Djako B, Keita M, Bisseyou Y, Esmel A, Megnassan E. Computer-assisted Design of Novel Polyketide Synthase 13 of *Mycobacterium tuberculosis* Inhibitors Using Molecular Modeling and Virtual Screening. Journal of Pharmaceutical Research International. 2022; 34 (56): 12-41. https://doi.org/10.9734/jpri/ 2022/v34i567250

27 Shirude PS, Madhavapeddi P, Naik M, Murugan K, Shinde V, Nandishaiah R, Bhat J, Kumar A, Hameed S, Holdgate G, Davies G, McMiken H, Hegde N, Ambady A, Venkatraman J, Panda M, Bandodkar B, Sambandamurthy VK, Read JA. Methyl-thiazoles: a novel mode of inhibition with the potential to develop novel inhibitors targeting InhA in Mycobacterium tuberculosis. J. Med. Chem. 2013; 56(21): 8533–42. https://doi.org/10.1021/jm4012033

28 Šink R, Sosič I, Živec M, Menendez R, Turk S, Pajk S, Gomez D, Roman E, Cortez C, Triconado J, Barturen I, Barros D, Pages L, Young R, Encinas L, Gobec S. Design, Synthesis, and Evaluation of New Thiadiazole-Based Direct Inhibitors of Enoyl Acyl Carrier Protein Reductase (InhA) for the Treatment of Tuberculosis. J. Med. Chem. 2014;58(2):613–24 https://doi.org/10.1021/jm501029r

29 Berman HM, Westbrook J, Feng Z, Gilliland G, Bhat TN, Weissig H, Shindyalov IN, Bourne PE. The protein data bank. Nucleic Acids Res. 2000; 28(1): 235–42. https://doi.org/10.1093/nar/28.1.235

30 Insight-II. Insight-II and Discover Molecular Modeling and Simulation Package, version. San Diego: Accelrys, Incorp; 2005.

31 BekonoBD, Esmel AE, Dali B, Ntie-Kang F, Keita M, Owono LCO. and Megnassan E. Computer-Aided Design of Peptidomimetic Inhibitors of Falcipain-3: QSAR and Pharmacophore Models. *Sci.*

Pharm. 2021, *89*(4),*44;* https://doi.org/10.3390/scipharm89040044

32 N'Guessan H, Megnassan E. In silico design of phosphonic arginine and hydroxamic acid inhibitors of Plasmodium falciparum M17 Leucyl aminopeptidase with favorable pharmacokinetic profile. J. Drug Des. Med. Chem. 2017;3(6): 98–125. https://doi.org/10.11 648/j.jddmc.20170306.13

33 Allangba KNPG, Keita M, Kre N'Guessan R, Megnassan E, Frecer V, Miertus S. Virtual design of novel Plasmodium falciparum cysteine protease falcipain-2 hybrid lactone-chalcone and isatin-chalcone inhibitors probing the S2 active site pocket. J. Enz. Inhib. Med. Chem. 2019; 34(1): 547–61. https://doi.org/10.1080/ 14756366.2018.1564288

34 Adama N, N'Guessan H, Dali B, Megnassan E. Computer-Assisted Design of Hydroxamic Acid Derivatives Inhibitors of M1 Metallo Aminopeptidase of *Plasmodium falciparum* with Favorable Pharmaco-kinetic Profile. J. Pharm. Res. Int. 2022; 34(60): 21-44. https://doi.org/10.9734/JPRI/2022/v34i607271

35 Dali B, Keita M, Megnassan E, Frecer V, Miertus S. Insight into selectivity of peptidomimetic inhibitors with modified statine core for plasmepsin II of Plasmodium falciparum over human Cathepsin D. Chem. Biol. Drug Des. 2012; 79(4): 411–30. https://doi.org/10.1111/j.1747-0285.2011.01276.x

36 Esmel A, Keita M, Megnassan E, Beguemsi T, Frecer V, Miertus S. Insight into binding mode of nitrile inhibitors of Plasmodium falciparum falcipain-3, QSAR and pharmacophore models, virtual design of new analogues with favorable pharmacokinetic profiles. J. Comput. Chem. Mol. Model. 2017; 2(1): 103–24. http://www.dx.doi.org/10.25177/JCMP.2.1.5

37 Megnassan E, Keita M, Bieri C, Esmel A, Frecer V, Miertus S. Design of novel dihydroxynaphthoic acid inhibitors of *Plasmodium Falciparu*m Lactate Dehydrogenase. Med. Chem. 2012; 8(5): 970–84. https://doi:10.2174/157340612802084324

38 Maple JR, Hwang MJ, Stockfisch TP, Dinur U, Waldman M, Ewig C, Hagler A. Derivation of class II force fields. I. Methodology and quantum force field for the alkyl functional group and alkane molecules. J. Comput. Chem. 1994; 15(2): 162–82. https://doi.org/10.1002/ jcc.540150207

39 Gilson MK, Honig B. The inclusion of electrostatic hydration energies in molecular mechanics calculations. J. Comput. Aid Mol. Des. 1991; 5(1): 5–20. https://doi.org/10.1007/BF00173467

40 Rocchia W, Sridharan S, Nicholls A, Alexov E, Chiabrera A, Honig B. Rapid grid-based construction of the molecular surface and the use of induced surface charge to calculate reaction field energies: applications to the molecular systems and geometric objects. J. Comput. Chem. 2002; 23(1): 128–37. https://doi.org/10.1002/jcc.1161

41 Bozzano GL. Theory of electric polarization. Dielectrics in Static Fields. 2nd Edition: Elsevier; 1973.

42 Discovery Studio Molecular Modeling and Simulation Program. version 2.5. San Diego: Accelrys, Incorp; 2009.

43 Li H, Sutter J, Hoffmann R. HypoGen: an automated system for generating 3D predictive pharmacophore models. Pharmacophore perception, development, and use in drug design. 2000; 2:171-89.

44 Owono Owono LC, Ntie-Kang F, Keita M, Megnassan E, Frecer V, Miertus S. Virtually designed triclosan-based inhibitors of enoyl-acyl carrier protein reductase of *Mycobacterium tuberculosis* and of *Plasmodium falciparum.* Mol. Inform. 2015; 34(5): 292–307. https://doi.org/10.1002/minf.201400141

45 Rozwarski DA, Vilcheze C, Sugantino M, Bittman R, Sacchettini JC. Crystal structure of the Mycobacterium tuberculosis enoyl-ACP reductase, InhA, in complex with NAD+ and a C16 fatty acyl substrate. J. Biol. Chem. 1999; 274(22): 15582–89. https://doi.org/10.1074/ jbc.274.22.15582

46 Bieri C,Esmel A, Keita M, Owono Owono LC,Dali B, Megnassan E, Frecer V, Miertus S. « Structure-Based Design and Pharmacophore-Based Virtual Screening of Combinatorial Library of Triclosan Analogues Active against Enoyl-Acyl Carrier Protein Reductase of *Plasmodium falciparum* with Favourable ADME Profiles », Int. J. Mol. Sci., vol. 24, no 8, p. 6916, avr. 2023, doi: 10.3390/ijms24086916

47 Sullivan TJ, Truglio JJ, Boyne ME, Novichenok P, Zhang X, Stratton C, Li HJ, Kaur T, Amin A, Johnson F. High affinity InhA inhibitors with activity against drug-resistant strains of Mycobacterium tuberculosis. ACS Chem. Biol. 2006; 1(1): 43–53. https://doi.org/ 10.1021/cb0500042

48 John S, Thangapandian S, Sakkiah S, Lee KW. Potent BACE-1 inhibitor desin using pharmacophore modeling, in silico screening and molecular docking studies. BMC Bioinform. 2011; 12(1): 28-38. https://bmcbioinformatics.biomedcentral.com/articles/10.1186/1471-2105-12-S1-S28

49 Frecer V, Megnassan E, Miertus S. Design and in silico screening of combinatorial library of antimalarial analogs of triclosan inhibiting Plasmodium falciparum enoyl-acyl carrier protein reductase. Eur. J. Med. Chem. 2009; 44(7):3009–19. https://doi.org/10.1016/j.ej mech.2008.12.028

50 Lipinski CA, Lombardo F, Dominy BW, Feeney PJ. Experimental and computational approaches to estimate solubility and permeability in drug discovery and development settings. Adv. Drug Deliv. Rev. 2001; 46(1-3): 3–26. https://doi.org/0.1016/s0169-409x (00)00129-0

51 Schrödinger. QikProp, 6.5 (Release 139); Schrödinger LLC: New York, NY, USA, 2019.

52 Jorgensen WL, Duffy EM. Prediction of drug solubility from Monte Carlo simulations. Bioorg. Med. Chem. Lett. 2000; 10(11): 1155–58. https://doi.org/10.1016/ s0960-894x(00)00172-4

53 Jorgensen WL, Duffy EM. Prediction of drug solubility from structure. Adv. Drug Deliv. Rev. 2002; 54(3): 355–66. https://doi.org/10.1016/s0169-409x(02)00008-x

54 Frecer V, Berti F, Benedetti F, Miertus S. Design of peptidomimetic inhibitors of aspartic protease of HIV-1 containing –Phe-Psi-Pro– core and displaying favourable ADME-related properties. J. Mol. Graph. Model. 2008; 27(3): 376-87. https://doi.org/10.1016/ j.jmgm.2008.06.006